**ORIGINAL ARTICLE**

# A New Water-Based $^{87}$Sr/$^{86}$Sr Isoscape Map of Central and NE Germany, with Special Emphasis on Mountainous Regions

A. Käßner[1] · H. T. Kalapurakkal[1,2] · B. Huber[3] · M. Tichomirowa[1]

## Abstract

In this study, we present a new $^{87}$Sr/$^{86}$Sr isoscape map of Central and NE Germany. This area is characterized by an alternation of sedimentary basins and mountainous regions with a very variable lithology. Since lithology and rock age have a major impact on the isotopic composition of biologically available strontium, Central and NE Germany should reveal highly variable $^{87}$Sr/$^{86}$Sr ratios. From lithological characteristics, particularly high ratios are expected in the mountainous regions of the Erzgebirge/Fichtelgebirge and the Harz Mountains. In contrast to these predictions, published $^{87}$Sr/$^{86}$Sr isoscape maps of Central and NE Germany record rather uniform and low $^{87}$Sr/$^{86}$Sr ratios. From this observation, we suspected that existing isoscape maps might be computed from an insufficient database, with mountainous regions being underrepresented. Our goal was to gather $^{87}$Sr/$^{86}$Sr baselines for each major lithology of Central and NE Germany and to produce an accurate isoscape map of Central and NE Germany. In the first step, we evaluated the suitability of stream water and groundwater as a proxy for biologically available strontium. In a selected watershed, we present mixing relationships and a stream network model. We show that groundwater is prone to very local geologic and anthropogenic influences and should thus be avoided. Instead, we focussed our further sampling on stream water. Altogether, we used 119 new measurements of groundwater and stream water and a set of 23 auxiliary variables as a database for our new isoscape map of Central and NE Germany. Due to a sampling strategy that focussed on covering each major lithology, our measurements and the final isoscape map show a clear contrast between sedimentary basins and mountainous regions. For regions that have been sufficiently sampled, a direct comparison of the isoscape map with published and new data shows good agreement. Although Central and NE Germany were part of published isoscape maps, our new map is the first that predicts $^{87}$Sr/$^{86}$Sr ratios in mountainous regions with high accuracy.

B. Huber: Freelancing in various machine learning projects and as university lecturer (http://www.biancahuber.de).

✉ A. Käßner
   alexandra.kaessner@mineral.tu-freiberg.de

1   Institut für Mineralogie, TU Bergakademie Freiberg, Brennhausgasse 14, 09599 Freiberg, Sachsen, Germany

2   Geomar Helmholtz Centre for Marine Research, Kiel, Germany

3   Freiberg, Germany

# 1 Introduction

Isoscape (isotope landscape) maps predict the spatial distribution of isotope ratios that contain geographic information, like e.g. strontium, sulphur, hydrogen, or oxygen (West et al. 2010). Since strontium isotopes are not fractionated by metabolic processes when incorporated into living organisms through water or food consumption, they are of particular interest. Isoscape maps of $^{87}Sr/^{86}Sr$ can thus be used directly for archaeological or animal migration studies without additional fractionation correction (e.g. Price et al. 2002; Bentley 2006; Bataille et al. 2021). Additionally, strontium isotope ratios ($^{87}Sr/^{86}Sr$) may vary over short distances because they are largely influenced by the local geological setting (e.g. Beard and Johnson 2000; Bentley 2006; Voerkelius et al. 2010; Bataille et al. 2014). Thus, provenance assignments based on strontium isotopes can reach a relatively high resolution.

Although rocks are the main source of strontium in the environment, provenance studies have to consider the isotopic composition of biologically available strontium, which may differ significantly from the values of the local lithology (e.g. Price et al. 2002). These differences arise from the differential weathering of minerals and from the addition of strontium from other sources such as dust, sea salt deposition, or fertilizers (Böhlke and Horan 2000; Zieliński et al. 2018; Bataille et al. 2018; Thomsen and Andreasen 2019).

Thus, a representative database of measured $^{87}Sr/^{86}Sr$ ratios is necessary to produce accurate isoscape maps (Bataille et al. 2020; Holt et al. 2021). To obtain this database, many strontium isotope studies rely on a suite of different samples like soil leachates, small animal tissue, plants, surface water, and groundwater (e.g. Bataille et al. 2018; Ladegaard-Pedersen et al. 2020). While some studies argue that single materials may not reflect the strontium variability as close as a combination of different archives (Crowley et al. 2017; Grimstead et al. 2017), the inter-site variation typically exceeds intra-site variations (Podio et al. 2013; Ladegaard-Pedersen et al. 2020). This advocates the use of only one single material to compute an isoscape map of $^{87}Sr/^{86}Sr$, as done by some researchers (e.g. Hoogewerff et al. 2019; Scaffidi et al. 2020). Such an approach allows focusing on a broad and representative sampling strategy to optimally cover the spatial variability of $^{87}Sr/^{86}Sr$.

For the generation of isoscape maps from a database of measured $^{87}Sr/^{86}Sr$ ratios, machine learning algorithms have recently been preferred over all other interpolation methods (e.g. Bataille et al. 2020; Holt et al. 2021). A major advantage of these algorithms is that a relatively small dataset of measured $^{87}Sr/^{86}Sr$ ratios can be used to train the algorithm to calculate high-resolution isoscape maps from a bundle of auxiliary variables (Bataille et al. 2018, 2020). Auxiliary variables are maps of factors that potentially influence $^{87}Sr/^{86}Sr$ ratios. Lithology, rock age, sea salt deposition, evapotranspiration, and aridity are typical factors of high impact in isoscape map calculations of Central Europe (Bataille et al. 2018; Hoogewerff et al. 2019). Bataille et al. (2018) tested different machine learning algorithms and showed that random forest regression outperforms many other methods such as support vector machines, neural networks, or ordinary kriging.

In Central and NE Germany, the surface geology is characterized by an alternation of sediment-filled basins and geologically complex mountainous regions (Fig. 1). These two types of regions should result in distinct $^{87}Sr/^{86}Sr$ ratios. For mountainous regions (like the Erzgebirge/Fichtelgebirge, the Harz Mountains, the Lusatian Block, the Thuringian-Franconian Slate Belt, the Thuringian Forest Basin, the Chemnitz Basin, the Granulite Mountains, and the North Saxon Volcanic complex, Fig. 1b, c) with prevalent Precambrian and Palaeozoic granitic gneisses, granites, rhyolites and clastic sediments, highly radiogenic and variable $^{87}Sr/^{86}Sr$ ratios are suggested. In difference, lower and more homogeneous
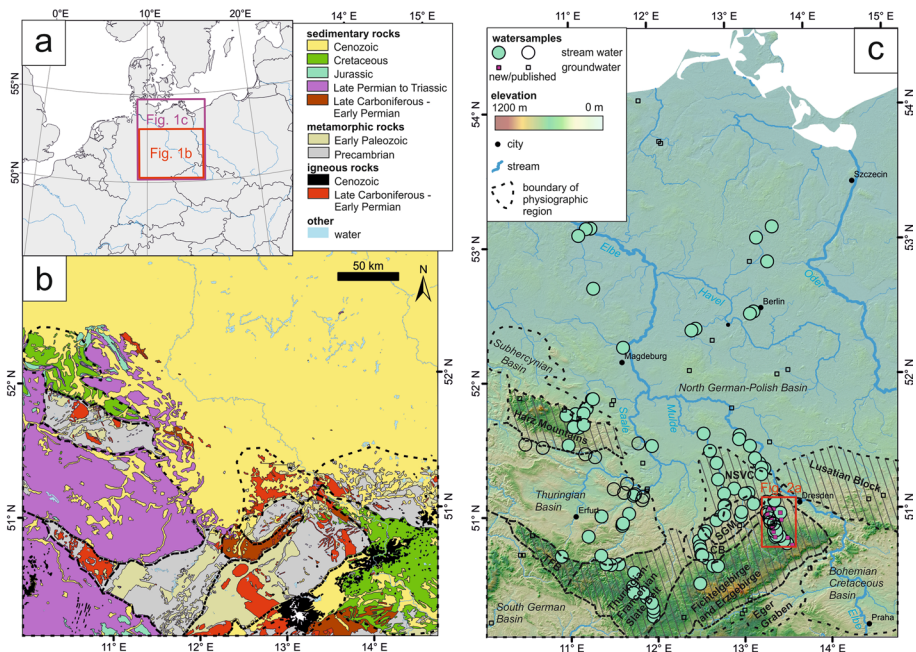
**Fig. 1** Geological and geographical setting with sample locations. **a** Map of Central Europe with land masses (grey), ocean (white), national borders (black lines), and major streams (blue) **b** Geological overview map of Central and NE Germany showing the distribution of different rock types based on the Geological Map of Germany 1: 1,000,000 (BGR, 2014). Nine major rock types were defined based on their formation type (sedimentary, metamorphic, igneous rocks) and their ages (e.g. Cenozoic, Cretaceous, Jurassic, and other) **c** Elevation map of Central and NE Germany with location and type of water samples. Hollow symbols mark previously published data (Voerkelius et al. 2010; Tichomirowa et al. 2010; Maurer et al. 2012), filled symbols mark new samples. The streams were extracted from SRTM DEM (Jarvis et al. 2008), which is shown as a shaded relief map. Mountainous regions are marked with hatched lines. All regions without hatching are sedimentary basins. Abbreviations of regions are: NSVC—North Saxon Volcanic Complex, SGM—Saxon Granulite Mountains, CB—Chemnitz Basin, TFB—Thuringian Forest Basin

$^{87}$Sr/$^{86}$Sr ratios are expected in carbonate-bearing Meso- and Cenozoic sediments in the Thuringian Basin, the North German Basin, the Czech Eger Graben, the Bohemian Cretaceous Basin, and the Subhercynian Basin (Fig. 1b, c).

In recently published $^{87}$Sr/$^{86}$Sr isoscape maps of Central and NE Germany, a clear difference between sedimentary basins and mountainous regions in Central- and NE Germany is not observable (Hoogewerff et al. 2019) or seems to be underestimated (Bataille et al. 2018). Hoogewerff et al. (2019) predicted uniform and low ratios (around 0.705) for entire Central and NE Germany from soil leachate $^{87}$Sr/$^{86}$Sr data. In contrast, the map of Bataille et al. (2018) predicted differences between mountainous regions (around 0.710 to 0.715) and sediment-filled basins (< 0.710). While the modelled values in sediment-filled basins are in agreement with previous published data (Voerkelius et al. 2010; Maurer et al. 2012) the mountainous region of the Erzgebirge should be characterized by ratios up to 0.720 (Voerkelius et al. 2010; Tichomirowa et al. 2010). A variety of other mountainous regions in Central and NE Germany (the Harz Mountains, the Lusatian Block, the Thuringian-Franconian Slate Belt, the Thuringian Forest Basin, the Chemnitz Basin, the Granulite Mountains, and the North Saxon Volcanic complex) is not represented by published samples (Fig. 1c) or $^{87}$Sr/$^{86}$Sr isoscape maps.

In this study, we designed a sampling strategy that is adapted to complex geological settings. We present a dataset of 119 new $^{87}$Sr/$^{86}$Sr ratios of water samples from Central and NE Germany and compare the suitability of surface water and groundwater as a proxy for the biologically available $^{87}$Sr/$^{86}$Sr ratio. In a second step, we used two different approaches to model $^{87}$Sr/$^{86}$Sr isoscape maps from these data. Because of the dense sampling and the stream network-related sampling strategy, we were able to compute a dendritic model of the strontium isotopic composition of the Freiberger Mulde catchment according to the approach of Brennan et al. (2016). Finally, we used the complete $^{87}$Sr/$^{86}$Sr dataset to produce an isoscape map of Central and NE Germany by applying the machine learning approach of Bataille et al. (2018), which uses random forest regression to compute an isoscape map from the strontium isotopic composition of the samples and a bundle of auxiliary variables. A comparison with existing isoscape maps of Central Europe highlights the advantages and disadvantages of small-scale and large-scale isoscape maps in migration studies.

## 2 Materials and Methods

### 2.1 Sampling Approach

The small sub-catchment of the Freiberger Mulde (Eastern Erzgebirge) has a very diverse lithology where Paleozoic gneisses and phyllites alternate with granites, volcanic dykes, but also with some Cretaceous sediments. In addition, numerous hydrothermal and mineral deposits occur in this region (Hoth et al. 1995; Rohde 2014; Fig. 2a). To understand the impact of small-scale lithological changes on $^{87}$Sr/$^{86}$Sr, we took 31 closely spaced samples and determined their strontium isotopic composition and concentration. Additionally, we measured physico-chemical parameters (temperature, pH, electrical conductivity, redox potential, and dissolved oxygen) during sample collection. With the parallel sampling of stream water and groundwater (Fig. 2a), we aimed to define the most appropriate type of water samples.

Because of the complex geological setting in Central and NE Germany, $^{87}$Sr/$^{86}$Sr ratios of stream water may change over short distances. We distinguished nine major lithological rock types based on their formation (sedimentary, metamorphic, igneous) and their ages (e.g. Cenozoic, Cretaceous, Jurassic and others, compare Fig. 1b). From prevalent rock types, we defined 14 geologically uniform and coherent regions (Fig. 1b, c). In most cases, these regions correspond to common physiographic regions of Central and NE Germany.

From each physiographic region, we took water samples to cover the entire range of $^{87}$Sr/$^{86}$Sr ratios. In particular, we sampled several traverses along streams that flow from mountainous regions into sedimentary basins to trace $^{87}$Sr/$^{86}$Sr changes (Fig. 1c). Altogether, we collected 119 water samples during the summer and early fall from 2016 to 2020 (Table 1). Around 50 ml of sediment-free water from each location was sampled and categorized as groundwater (from wells/springs) or stream water (Table 1, Fig. 1c).

### 2.2 Strontium Isotope Analysis Methods

Water samples were prepared for analysis in the Isotope Geochemistry and Geochronology Lab at TU Bergakademie Freiberg, Institute of Mineralogy. For strontium isotopic
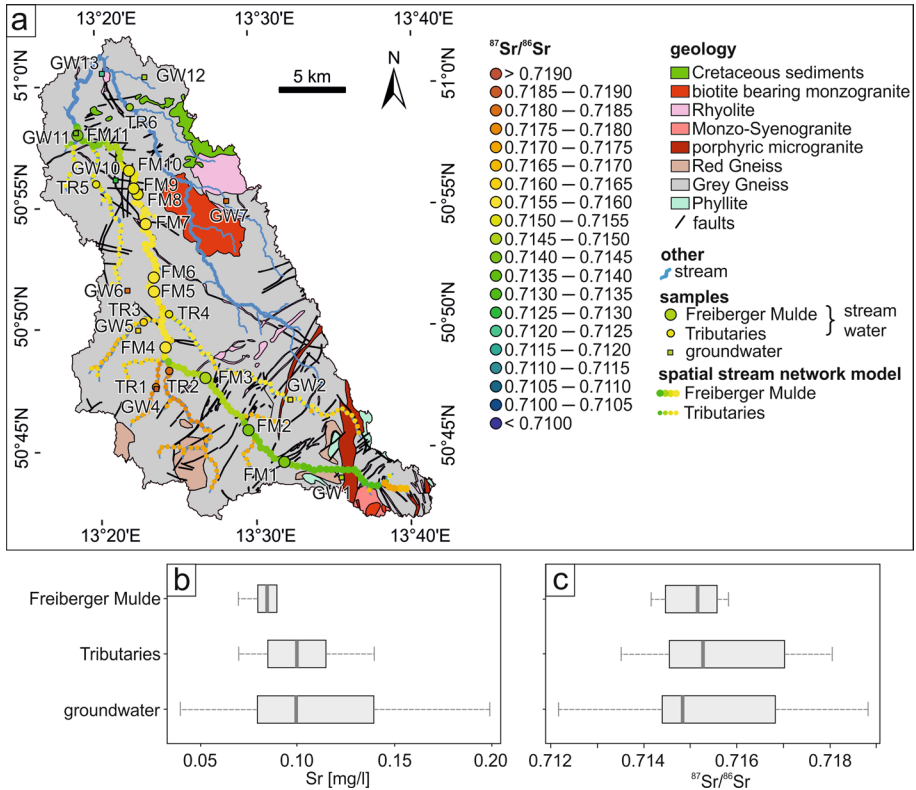
**Fig. 2** Strontium isotopic composition and strontium concentration of the Freiberger Mulde (FM), its tributaries (TR) and groundwater (GW) in the Freiberger Mulde catchment. The general flow direction is from South to North. **a** Catchment area of the Freiberger Mulde river (see location in Fig. 1c) showing the distribution of different rock types together with measured strontium isotopic composition for stream water and groundwater samples (filled circles and squares, respectively) compared to results of spatial stream network modelling (shown as coloured points along streams; colours correspond to the legend). FM: samples from Freiberger Mulde, TR–samples from tributaries, GW – groundwater samples. The streams were extracted from SRTM DEM (Jarvis et al. 2008). **b** Box plots comparing the strontium concentration of the main stream (Freiberger Mulde), its tributaries and groundwater from the Freiberger Mulde catchment. **c** Box plots comparing the $^{87}Sr/^{86}Sr$ ratios of the Freiberger Mulde, its tributaries and groundwater from the Freiberger Mulde catchment

composition determination ca. 30 ml of water was evaporated overnight at 85 °C. For the strontium concentration determination weighed aliquots of 7 ml were mixed with a known quantity of a calibrated $^{84}Sr$-enriched spike solution. The mixed solution was also evaporated at 85 °C. Afterwards, the precipitates were re-dissolved in 0.5 ml of 3.5 N $HNO_3$ for column chemistry. Strontium was separated from the matrix through cation exchange chromatography using 0.2 ml teflon columns with Sr-Spec cation exchange resins (Charlier et al. 2006) and loaded onto pre-degassed W-filaments. Strontium isotope ratios were measured on the Finnigan MAT 262 thermal ionization mass spectrometer (TIMS, Thermo Fischer Scientific) at TU Bergakademie Freiberg. During measurements, the $^{87}Sr/^{86}Sr$ ratio was corrected for mass fractionation using an exponential law, normalizing to $^{86}Sr/^{88}Sr = 0.1194$. The standard NBS987 was analysed repeatedly during measurements and yielded an average $^{87}Sr/^{86}Sr$ ratio of $0.71023 \pm 0.00003$ (n = 12). This is within

**Table 1** Strontium isotope ratios and strontium concentrations of water samples collected from 119 locations in NE Germany

| Sample | Latitude | Longitude | Water body | Category | Geological terrane | $^{87}Sr/^{86}Sr$ | Strontium concentration [µg/l] |
|---|---|---|---|---|---|---|---|
| *Freiberger Mulde catchment* | | | | | | | |
| FM1 | 50.96686 | 13.31326 | Freiberger Mulde | Stream water | Erzgebirge and Fichtelgebirge | 0.71395 | 66.2 |
| FM2 | 50.76292 | 13.49214 | Freiberger Mulde | Stream water | Erzgebirge and Fichtelgebirge | 0.71447 | n.a |
| FM3 | 51.13022 | 13.09338 | Freiberger Mulde | Stream water | Erzgebirge and Fichtelgebirge | 0.71281 | 85.5 |
| FM4 | 51.16627 | 12.92405 | Freiberger Mulde | Stream water | Erzgebirge and Fichtelgebirge | 0.71326 | 82.5 |
| FM5 | 50.86672 | 13.39114 | Freiberger Mulde | Stream water | Erzgebirge and Fichtelgebirge | 0.71638 | 92 |
| FM6 | 50.86858 | 13.39308 | Freiberger Mulde | Stream water | Erzgebirge and Fichtelgebirge | 0.71557 | n.a |
| FM7 | 50.90528 | 13.38528 | Freiberger Mulde | Stream water | Erzgebirge and Fichtelgebirge | 0.71565 | 92.4 |
| FM8 | 50.92583 | 13.37722 | Freiberger Mulde | Stream water | Erzgebirge and Fichtelgebirge | 0.71542 | n.a |
| FM9 | 50.92972 | 13.37306 | Freiberger Mulde | Stream water | Erzgebirge and Fichtelgebirge | 0.71547 | n.a |
| FM10 | 50.94194 | 13.36833 | Freiberger Mulde | Stream water | Erzgebirge and Fichtelgebirge | 0.71546 | n.a |
| FM11 | 50.74066 | 13.53016 | Freiberger Mulde | Stream water | Erzgebirge and Fichtelgebirge | 0.71415 | n.a |
| FM12 | 51.06023 | 13.30385 | Freiberger Mulde | Stream water | Erzgebirge and Fichtelgebirge | 0.71328 | 81.5 |
| TR1 | 50.79356 | 13.39308 | Freiberger Mulde | Stream water | Erzgebirge and Fichtelgebirge | 0.71791 | 74.5 |
| TR2 | 50.80453 | 13.40799 | Freiberger Mulde | Stream water | Erzgebirge and Fichtelgebirge | 0.71804 | 72.1 |
| TR3 | 50.83811 | 13.38109 | Freiberger Mulde | Stream water | Erzgebirge and Fichtelgebirge | 0.71614 | 120 |
| TR4 | 50.84332 | 13.40886 | Freiberger Mulde | Stream water | Erzgebirge and Fichtelgebirge | 0.71523 | 96 |
| TR5 | 50.93315 | 13.33235 | Freiberger Mulde | Stream water | Erzgebirge and Fichtelgebirge | 0.71527 | 112 |
| TR6 | 50.98545 | 13.37026 | Freiberger Mulde | Stream water | Erzgebirge and Fichtelgebirge | 0.71351 | 137 |
| TR7 | 50.97308 | 13.46361 | Freiberger Mulde | Stream water | Erzgebirge and Fichtelgebirge | 0.71388 | 103 |
| GW1 | 50.72910 | 13.59156 | Groundwater Freiberg | Groundwater | Erzgebirge and Fichtelgebirge | 0.71459 | 38.9 |
| GW2 | 50.78321 | 13.53803 | Groundwater Freiberg | Groundwater | Erzgebirge and Fichtelgebirge | 0.71506 | 72 |
| GW4 | 50.79348 | 13.39345 | Groundwater Freiberg | Groundwater | Erzgebirge and Fichtelgebirge | 0.71881 | 87.8 |
| GW5 | 50.83250 | 13.37500 | Groundwater Freiberg | Groundwater | Erzgebirge and Fichtelgebirge | 0.71641 | 105 |
| GW6 | 50.85995 | 13.36421 | Groundwater Freiberg | Groundwater | Erzgebirge and Fichtelgebirge | 0.71827 | 171 |

**Table 1** (continued)

| Sample | Latitude | Longitude | Water body | Category | Geological terrane | $^{87}Sr/^{86}Sr$ | Strontium concentration [µg/l] |
|---|---|---|---|---|---|---|---|
| GW7 | 50.91994 | 13.47260 | Groundwater Freiberg | Groundwater | Erzgebirge and Fichtelgebirge | 0.71682 | 144 |
| GW10 | 50.93551 | 13.35355 | Groundwater Freiberg | Groundwater | Erzgebirge and Fichtelgebirge | 0.71287 | 108 |
| GW11 | 50.96830 | 13.31157 | Groundwater Freiberg | Groundwater | Erzgebirge and Fichtelgebirge | 0.71439 | 68.5 |
| GW12 | 51.00582 | 13.38693 | Groundwater Freiberg | Groundwater | Erzgebirge and Fichtelgebirge | 0.71463 | 163 |
| GW13 | 51.00871 | 13.34087 | Groundwater Freiberg | Groundwater | Erzgebirge and Fichtelgebirge | 0.71216 | 112 |
| GW14 | 50.97317 | 13.46316 | Groundwater Freiberg | Groundwater | Erzgebirge and Fichtelgebirge | 0.71397 | 86.1 |
| GW15 | 50.97411 | 13.46534 | Groundwater Freiberg | Groundwater | Erzgebirge and Fichtelgebirge | 0.71768 | 196 |
| *Central and NE Germany* | | | | | | | |
| CHE1 | 50.97129 | 12.79675 | Chemnitz | Stream water | Saxon Granulite Mountains | 0.71186 | n.a |
| DA1 | 51.38972 | 13.18504 | Dahle | Stream water | Bohemian Cretaceous Basin | 0.71112 | n.a |
| DAN1 | 53.08737 | 11.08350 | Jeetzel | Stream water | North German Basin | 0.71008 | n.a |
| DÖL1 | 51.31719 | 13.26258 | Döllnitz | Stream water | Bohemian Cretaceous Basin | 0.71081 | n.a |
| ELB1 | 51.56745 | 13.00951 | Elbe | Stream water | North German Basin | 0.71087 | n.a |
| ELB2 | 51.48454 | 13.13157 | Elbe | Stream water | North German Basin | 0.71097 | n.a |
| ELB3 | 51.35245 | 13.23758 | Elbe | Stream water | Bohemian Cretaceous Basin | 0.71112 | n.a |
| ELB4 | 51.31153 | 13.29342 | Elbe | Stream water | Bohemian Cretaceous Basin | 0.71114 | n.a |
| ELB5 | 53.14173 | 11.23632 | Elbe | Stream water | North German Basin | 0.70919 | n.a |
| ELB6 | 53.13772 | 11.17950 | Elbe | Stream water | North German Basin | 0.70949 | n.a |
| FM3 | 50.79923 | 13.44696 | Freiberger Mulde | Stream water | Erzgebirge and Fichtelgebirge | 0.71475 | n.a |
| FM4 | 50.82058 | 13.40431 | Freiberger Mulde | Stream water | Erzgebirge and Fichtelgebirge | 0.71583 | n.a |
| FM5* | 50.85902 | 13.39300 | Freiberger Mulde | Stream water | Erzgebirge and Fichtelgebirge | 0.71555 | n.a |
| GÖTT1 | 51.53540 | 9.91895 | Leine | Stream water | Thuringian Basin | 0.70826 | n.a |
| GT1 | 51.53650 | 13.00302 | Kuhteich in Torgau | Stream water | North German Basin | 0.70977 | n.a |
| HARZ1 | 51.66813 | 11.13340 | Selke | Stream water | Harz Mountains | 0.71204 | n.a |

**Table 1** (continued)

| Sample | Latitude | Longitude | Water body | Category | Geological terrane | $^{87}Sr/^{86}Sr$ | Strontium concentration [µg/l] |
|---|---|---|---|---|---|---|---|
| HARZI0 | 51.86159 | 11.24575 | Selke | Stream water | Subhercynian Basin | 0.70933 | n.a |
| HARZI1 | 51.85935 | 11.23327 | Bode | Stream water | Subhercynian Basin | 0.71027 | n.a |
| HARZ2 | 51.64751 | 11.07006 | Uhlenbach | Stream water | Harz Mountains | 0.71402 | n.a |
| HARZ3 | 51.65096 | 11.00972 | Elbingstalbach | Stream water | Harz Mountains | 0.71287 | n.a |
| HARZ4 | 51.73861 | 10.92198 | Bode | Stream water | Harz Mountains | 0.71170 | n.a |
| HARZ5 | 51.73885 | 10.92211 | Zufluss zu Bode | Stream water | Harz Mountains | 0.71167 | n.a |
| HARZ6 | 51.75078 | 11.03225 | Bode | Stream water | Harz Mountains | 0.71305 | n.a |
| HARZ7 | 51.75407 | 11.12999 | Quarmbach | Stream water | Subhercynian Basin | 0.71586 | n.a |
| HARZ8 | 51.79065 | 11.15993 | Bode | Stream water | Subhercynian Basin | 0.71079 | n.a |
| HARZ9 | 51.79037 | 11.16958 | Bicklingsbach | Stream water | Subhercynian Basin | 0.70904 | n.a |
| HOF1 | 50.32399 | 11.91403 | Saale | Stream water | Thuringian-Franconian Slate Belt | 0.71089 | n.a |
| HVL1 | 52.37584 | 12.51294 | Sandfurtgraben | Stream water | North German Basin | 0.71045 | n.a |
| HVL2 | 52.36460 | 12.46437 | Buckau | Stream water | North German Basin | 0.71058 | n.a |
| JAH1 | 51.26836 | 13.25655 | Jahna | Stream water | Bohemian Cretaceous Basin | 0.71021 | n.a |
| Jena1 | 50.90687 | 11.57920 | Leutra | Stream water | Thuringian Basin | 0.70800 | n.a |
| Jena2 | 50.92274 | 11.58463 | small stream | Stream water | Thuringian Basin | 0.70801 | n.a |
| KGRO | 51.03485 | 12.80108 | Sandgrube Biesern | Stream water | Saxon Granulite Mountains | 0.71150 | n.a |
| LUB1 | 50.83281 | 12.55180 | Lungwitzbach | Stream water | Chemnitz Basin | 0.71283 | n.a |
| MAGD1 | 52.24580 | 11.62275 | Ohre | Stream water | North German Basin | 0.71128 | n.a |
| RÖB1 | 50.67182 | 12.52188 | Rödelbach | Stream water | Erzgebirge and Fichtelgebirge | 0.71459 | n.a |
| RTLB1 | 51.51788 | 10.94528 | Schlossteich | Stream water | Harz Mountains | 0.70998 | n.a |
| Saa1 | 50.22159 | 11.93383 | Saale | Stream water | Thuringian-Franconian Slate Belt | 0.71381 | n.a |
| Saa10 | 50.99614 | 11.66418 | Heinze-Quelle | Stream water | Thuringian Basin | 0.71070 | n.a |
| Saa11 | 50.61855 | 11.53582 | Saale | Stream water | Thuringian-Franconian Slate Belt | 0.71094 | n.a |
| Saa12 | 50.61401 | 11.44198 | Saale | Stream water | Thuringian-Franconian Slate Belt | 0.71100 | n.a |

**Table 1** (continued)

| Sample | Latitude | Longitude | Water body | Category | Geological terrane | $^{87}Sr/^{86}Sr$ | Strontium concentration [µg/l] |
|---|---|---|---|---|---|---|---|
| Saal3 | 50.62022 | 11.38462 | Saale | Stream water | Thuringian-Franconian Slate Belt | 0.71117 | n.a |
| Saal4 | 51.50373 | 11.95203 | Saale | Stream water | Thuringian Basin | 0.70862 | n.a |
| Saa2 | 50.25832 | 11.93391 | Saale | Stream water | Thuringian-Franconian Slate Belt | 0.71346 | n.a |
| Saa3 | 50.28429 | 11.93322 | Ölsnitz | Stream water | Thuringian-Franconian Slate Belt | 0.70916 | n.a |
| Saa4 | 50.36575 | 11.85609 | Saale | Stream water | Thuringian-Franconian Slate Belt | 0.71149 | n.a |
| Saa5 | 50.40127 | 11.81649 | Saale | Stream water | Thuringian-Franconian Slate Belt | 0.71122 | n.a |
| Saa6 | 50.40185 | 11.70159 | Selbitz | Stream water | Thuringian-Franconian Slate Belt | 0.70910 | n.a |
| Saa7 | 50.44945 | 11.69617 | Saale | Stream water | Thuringian-Franconian Slate Belt | 0.71071 | n.a |
| Saa9 | 50.55268 | 11.71329 | Saale | Stream water | Thuringian-Franconian Slate Belt | 0.71069 | n.a |
| SAW1 | 52.69170 | 11.26250 | Moorgraben | Stream water | North German Basin | 0.71143 | n.a |
| SLM | 50.59212 | 12.64796 | Schlema | Stream water | Erzgebirge and Fichtelgebirge | 0.71545 | n.a |
| STR1 | 51.04723 | 13.14837 | Striegis | Stream water | Saxon Granulite Mountains | 0.71305 | n.a |
| SW1 | 50.58855 | 12.70301 | Schwarzwasser | Stream water | Erzgebirge and Fichtelgebirge | 0.71590 | n.a |
| THY1 | 51.51421 | 10.94658 | Thyra | Stream water | Harz Mountains | 0.71155 | n.a |
| TR1* | 51.06746 | 13.39975 | Triebisch | Stream water | Erzgebirge and Fichtelgebirge | 0.71168 | n.a |
| VM1 | 51.23947 | 12.73336 | Vereinigte Mulde | Stream water | North Saxon Volcanic Complex | 0.71346 | n.a |
| VM2 | 51.36368 | 12.72105 | Vereinigte Mulde | Stream water | North Saxon Volcanic Complex | 0.71357 | n.a |
| VM3 | 51.45633 | 12.64871 | Vereinigte Mulde | Stream water | North Saxon Volcanic Complex | 0.71350 | n.a |
| VM4 | 51.58692 | 12.57708 | Vereinigte Mulde | Stream water | North Saxon Volcanic Complex | 0.71364 | n.a |
| W1 | 53.12400 | 13.50100 | Templiner Kanal | Stream water | North German Basin | 0.71070 | n.a |
| W10 | 52.49100 | 13.23400 | Teufelsee | Stream water | North German Basin | 0.71037 | n.a |
| W11 | 52.47800 | 13.19000 | Havel | Stream water | North German Basin | 0.70968 | n.a |
| W2 | 53.04640 | 13.30000 | Burgwall | Stream water | North German Basin | 0.71046 | n.a |
| W3 | 52.86300 | 13.42600 | Liebenwalde | Stream water | North German Basin | 0.71042 | n.a |
| W4 | 50.67900 | 10.86000 | Ilm | Stream water | Thuringian Forest Basin | 0.71128 | n.a |

**Table 1** (continued)

| Sample | Latitude | Longitude | Water body | Category | Geological terrane | $^{87}Sr/^{86}Sr$ | Strontium concentration [µg/l] |
|--------|----------|-----------|------------|----------|--------------------|-----------|-----------------|
| W5 | 50.82900 | 11.17900 | Ilm | Stream water | Thuringian Basin | 0.70882 | n.a |
| W6 | 50.98000 | 11.33400 | Ilm | Stream water | Thuringian Basin | 0.70810 | n.a |
| W7 | 51.13200 | 11.72200 | Saale | Stream water | Thuringian Basin | 0.70872 | n.a |
| W8 | 50.92500 | 11.58900 | Saale | Stream water | Thuringian Basin | 0.70955 | n.a |
| W9 | 50.68500 | 11.32600 | Saale | Stream water | Thuringian Basin | 0.71072 | n.a |
| WEI1 | 50.97977 | 11.33376 | Ilm | Stream water | Thuringian Basin | 0.70827 | n.a |
| WEI2 | 50.97975 | 11.33441 | Leutra | Stream water | Thuringian Basin | 0.70794 | n.a |
| ZM1 | 51.13051 | 12.80255 | Zwickauer Mulde | Stream water | North Saxon Volcanic Complex | 0.71411 | n.a |
| ZM10 | 50.65002 | 12.57914 | Zwickauer Mulde | Stream water | Erzgebirge and Fichtelgebirge | 0.71616 | n.a |
| ZM11 | 50.58951 | 12.70003 | Zwickauer Mulde | Stream water | Erzgebirge and Fichtelgebirge | 0.71589 | n.a |
| ZM12 | 50.58785 | 12.70156 | Zwickauer Mulde | Stream water | Erzgebirge and Fichtelgebirge | 0.72313 | n.a |
| ZM2 | 51.04447 | 12.80775 | Zwickauer Mulde | Stream water | Saxon Granulite Mountains | 0.71355 | n.a |
| ZM3 | 50.96505 | 12.75711 | Zwickauer Mulde | Stream water | Saxon Granulite Mountains | 0.71455 | n.a |
| ZM4 | 50.93282 | 12.70209 | Zwickauer Mulde | Stream water | Saxon Granulite Mountains | 0.71429 | n.a |
| ZM5 | 50.85438 | 12.57197 | Zwickauer Mulde | Stream water | Chemnitz Basin | 0.71466 | n.a |
| ZM6 | 50.78212 | 12.48820 | Zwickauer Mulde | Stream water | Chemnitz Basin | 0.71498 | n.a |
| ZM7 | 50.74092 | 12.49349 | Zwickauer Mulde | Stream water | Chemnitz Basin | 0.71535 | n.a |
| ZM8 | 50.71774 | 12.50159 | Zwickauer Mulde | Stream water | Chemnitz Basin | 0.71578 | n.a |
| ZM9 | 50.67697 | 12.51022 | Zwickauer Mulde | Stream water | Erzgebirge and Fichtelgebirge | 0.71568 | n.a |
| ZSC1 | 51.12576 | 13.05018 | Zschopau | Stream water | Saxon Granulite Mountains | 0.71370 | n.a |
| ZSC2 | 50.95786 | 12.99290 | Zschopau | Stream water | Saxon Granulite Mountains | 0.71429 | n.a |
| ZSC3 | 50.98926 | 13.00483 | Zschopau | Stream water | Saxon Granulite Mountains | 0.71426 | n.a |

n.a.—not analysed; external reproducibility of $^{87}Sr/^{86}Sr$ is 0.00003, analytical error during measurement was lower than 0.00002

error equal to the published value of 0.71025 (Faure and Mensing 2005). Total procedural blanks were < 30 pg strontium, which is much lower than the amount of strontium in the samples and had no impact on our results.

## 2.3 Modelling of Isoscape Maps

### 2.3.1 *Modelling an $^{87}Sr/^{86}Sr$ baseline of the Freiberger Mulde catchment using spatial stream networks*

For the Freiberger Mulde catchment, we computed a spatial stream network model, which uses autocovariance structures to account for the spatial dependencies of river networks (Isaak et al. 2014; Brennan et al. 2016). We used all stream water sampling sites of the Freiberger Mulde catchment as input parameters (Fig. 2a, Table 1; n = 19) and adopted the modelling approach of Brennan et al. (2016) by using a geological map with eight different lithologies (the GLIM database, Hartmann and Moosdorf 2012, Fig. 2a) as an auxiliary variable. As suggested by Brennan et al. (2016), we used upstream and downstream autocorrelation and per cent geology as auxiliary variables.

In the Spatial Tools for the Analysis of River Systems (STARS) toolbox in ArcGIS 10.2 (Peterson and Ver Hoef 2014), a network topology free of geometric errors, a spatial stream network including the sampling and prediction points, the geological information as per cent geology for each sampling and prediction point, and spatial weights depending on the catchment size were prepared. The modelling itself was conducted in R using the spatial stream network (SSN) package (Ver Hoef et al. 2014) following the methodology of Brennan et al. (2016).

### 2.3.2 Modelling an Isoscape Map of Central and NE Germany by a Machine Learning Approach

To create a high-resolution isoscape map of Central and NE Germany, we used the machine learning approach of Bataille et al. (2018), which applies the caret package on R version 3.5.0 (Kuhn 2008). For this, we combined our new $^{87}Sr/^{86}Sr$ dataset with appropriate auxiliary variables (Table 2). Besides 20 auxiliary variables from different sources (Hijmans et al. 2005; Jarvis et al. 2008; Mooney et al. 2008; Potter et al. 2010; Balmino et al. 2012; Hartmann and Moosdorf 2012; Vet et al. 2014; Hengl et al. 2017; Börker et al. 2018; Mahowald et al. 2018; Table 2), predicted $^{87}Sr/^{86}Sr$ ratios of the published process-based bedrock model by Bataille et al. (2014) were included as their median (r.m1), first quartile (r.ssrq1), and third quartile (r.ssrq3). We extracted the auxiliary variable values for each geographical location to build the regression matrix and used it for training the spatial prediction model in the caret package (Kuhn 2008).

We applied the random forest regression model of Bataille et al. (2018) to the whole dataset and the auxiliary variables to create an $^{87}Sr/^{86}Sr$ isoscape map for Central and NE Germany. To assess the accuracy and precision of the model, the dataset was randomly split into a training subset (80% of the entire dataset) and a testing holdout subset for validation (20% of the total dataset). A comparison of observed vs. predicted $^{87}Sr/^{86}Sr$ ratios of training and testing datasets allows assessing the model performance.

**Table 2** List of climatic, geological, pedological, and topographic spatial data used as auxiliary variables (C = continuous; D = discrete)

| Variables | Description | Resolution | Type | Source |
|---|---|---|---|---|
| r.maxage_geol | GLiM age attribute (Myrs) | 1 km | D | Hartmann and Moosdorf (2012) |
| r.minage_geol | GLiM age attribute (Myrs) | 1 km | D | Hartmann and Moosdorf (2012) |
| r.meanage_geol | GLiM age attribute (Myrs) | 1 km | D | Hartmann and Moosdorf (2012) |
| r.age | Terrane age attribute (Myrs) | 1 km | D | Mooney et al. (2008) |
| r.GUM | Global unconsolidated sediment map | 1 km | C | Börker et al. (2018) |
| r.ssaw | Multi-models average sea salt wet deposition (kg ha$^{-1}$ year$^{-1}$) | 1°×1° | C | Vet et al. (2014) |
| r.ssa | Multi-models average | 1°×1° | C | Vet et al. (2014) |
| | Sea salt wet + dry deposition (kg ha$^{-1}$ year$^{-1}$) | | | |
| r.salt | CCSM.3 simulation (g m$^{-2}$ year$^{-1}$) | 1.4°×1.4° | C | Mahowald et al. (2018) |
| r.dust | Multi-models average (g m$^{-2}$ year$^{-1}$) | 1°×1° | C | Mahowald et al. (2018) |
| r.elevation | SRTM (m) | 90 m | C | Jarvis et al. (2008) |
| r.cec | Cation Exchange Capacity | 250 m | C | Hengl et al. |
| r.pet | Global Potential Evapotranspiration | 30-arc sec | C | Hengl et al. 2017 |
| r.ai | Global Aridity Index | 30-arc sec | C | Hengl et al. (2017) |
| r.ph | Soil pH in H2O solution (×10) | 250 m | C | Hengl et al. (2017) |
| r.clay | Clay (weight %) | 250 m | C | Hengl et al. (2017) |
| r.bulk | Bulk density (kg m$^{-3}$) | 250 m | C | Hengl et al. (2017) |
| r.bouguer | WGM2012_Bouguer | 2 min | C | Balmino et al. (2012) |
| r.map | Mean annual precipitation (mm year$^{-1}$) | 30-arc sec | C | Hijmans et al. (2005) |
| r.mat | Mean annual temperature (°C) | 30-arc sec | C | Hijmans et al. (2005) |
| r.fert | Global Nitrogen Fertilization | 30-arc sec | C | Potter et al. (2010) |
| r.m1 | Median bedrock model | 1 km | D | Bataille et al. (2018) |
| r.srsrq1 | Quartile 1 bedrock model | 1 km | D | Bataille et al. (2018) |
| r.srsrq3 | Quartile 3 bedrock model | 1 km | D | Bataille et al. (2018) |

To understand which of the auxiliary variables have the highest impact on the final model, we calculated IncNodePurity using the caret Package (Kuhn 2008) as a measure for variable importance.

# 3 Results

## 3.1 Water $^{87}$Sr/$^{86}$Sr Ratios of Central and NE Germany

The results of strontium analyses are given in Table 1. Figure 2 summarizes the results from 31 samples of the Freiberger Mulde river catchment. On-site parameters and strontium concentrations have been determined together with $^{87}$Sr/$^{86}$Sr ratios for these samples and are presented in Table 3. Two outliers were defined based on remarkably high electrical conductivity (Table 3). The $^{87}$Sr/$^{86}$Sr ratios and strontium concentrations of these samples were suspected to be influenced by anthropogenic contaminations and were excluded from Table 1 and the following interpretation and modelling.

Table 3 Physico-chemical parameters of surface- and subsurface waters of the upper Freiberger Mulde catchment

| Sample | T (°C) | pH | Ec (μS/cm) | Eh (mV) | DO (mg) | DO (%) |
|---|---|---|---|---|---|---|
| FM1 | 9.9 | 7.6 | 166 | 434 | 11.0 | 98 |
| FM2 | 10.1 | 7.5 | 203 | 458 | 11.0 | 101 |
| FM3 | 10.6 | 7.5 | 214 | 447 | 11.0 | 100 |
| FM4 | 11.2 | 7.8 | 220 | 433 | 11.0 | 100 |
| FM5 | 12.0 | 7.8 | 246 | 416 | 13.0 | 129 |
| FM6 | 11.6 | 7.9 | 241 | 433 | 9.9 | 95 |
| TR1 | 22.3 | 6.4 | 239 | 470 | 8.3 | 99 |
| TR2 | 10.5 | 7.5 | 215 | 451 | 12.0 | 110 |
| TR3 | 11.0 | 7.2 | 240 | 444 | 10.0 | 98 |
| TR4 | 10.8 | 7.4 | 209 | 449 | 13.0 | 124 |
| TR5 | 15.9 | 8.0 | 422 | 469 | 13.0 | 136 |
| TR6 | 12.3 | 7.9 | 335 | 447 | 13.0 | 138 |
| TR7 | 22.4 | 7.0 | 225 | 458 | 7.3 | 90 |
| GW1 | 22.1 | 6.0 | 109 | 528 | 7.6 | 91 |
| GW2 | 23.1 | 6.6 | 135 | 459 | 7.3 | 88 |
| GW3 | 21.5 | 6.6 | 150 | 464 | 7.1 | 84 |
| GW4 | 21.7 | 6.3 | 231 | 525 | 7.0 | 82 |
| GW5 | 12.3 | 5.4 | 165 | 485 | 9.1 | 90 |
| GW6 | 21.8 | 6.0 | 296 | 565 | 7.1 | 85 |
| GW7 | 22.7 | 6.1 | 255 | 517 | 7.3 | 87 |
| GW8* | 23.7 | 6.4 | 903 | 480 | 7.5 | 92 |
| GW9* | *23.1* | *6.0* | *903* | *481* | *8.1* | *99* |
| GW10 | 22.1 | 6.0 | 360 | 479 | 5.6 | 65 |
| GW11 | 21.9 | 5.4 | 294 | 495 | 6.7 | 80 |
| GW12 | 22.0 | 6.0 | 523 | 471 | 6.4 | 75 |
| GW13 | 22.0 | 3.6 | 690 | 571 | 7.2 | 85 |
| GW14 | 22.0 | 6.4 | 217 | 461 | 4.4 | 55 |
| GW15 | 22.9 | 4.9 | 235 | 517 | 7.3 | 94 |

Sample numbers with remarkably high electrical conductivity (Ec, marked with *) are suspected to be influenced by anthropogenic contaminations and were excluded from $^{87}Sr/Sr^{86}$ and strontium concenctration analysis

In the Freiberger Mulde catchment, the $^{87}Sr/^{86}Sr$ ratios range from 0.71216 to 0.71881, with a mean of 0.71536. We grouped the Freiberger Mulde dataset into samples from the main stream (FM, Freiberger Mulde), samples from tributaries (TR) and groundwater samples (GW) from springs and wells. The grouped strontium isotopic composition and concentration data are presented in Fig. 2b and c. In entire Central and NE Germany, $^{87}Sr/^{86}Sr$ ratios range from 0.70794 to 0.72313, with a mean of 0.71279.

## 3.2 Spatial Stream Network Model of the Freiberger Mulde Catchment

For a part of the Freiberger Mulde catchment, our sampling covered both the topological variation of the stream network and the lithological variation. This is the requirement to model the data in a spatial stream network (Brennan et al. 2016). The result of this modelling is shown in Fig. 2a, together with the measured $^{87}Sr/^{86}Sr$ ratios.
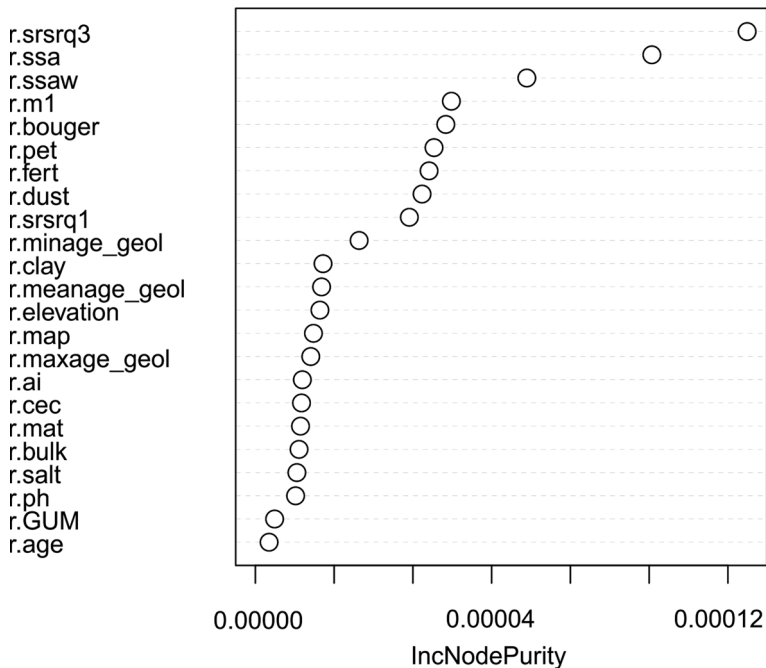
**Fig. 3** Variable importance plot for the isoscape map. IncNodePurity is used as a measure for the impact of each auxiliary variable on the final model, as suggested by Bataille et al. (2018). Abbreviations are explained in Table 2

### 3.3 Strontium Isoscape Map of Central and NE Germany

We computed our final isoscape map from 23 auxiliary variables and 119 new $^{87}Sr/^{86}Sr$ data from water. The relative impact of the single auxiliary variables on our model is summarized in Fig. 3. The resulting isoscape map of Central and NE Germany is presented together with the data in Fig. 4a. In Fig. 4b, we present four swath profiles of the $^{87}Sr/^{86}Sr$ ratios across the isoscape map. The swath profiles were derived from the final isoscape map using SAGA (Conrad et al. 2015). In swath profile analysis, the values are not only derived from the defined profile line, but also sampled in a specified width (swath width) perpendicular to the profile. From this dataset, mean, maximum and minimum values can be defined at each point along the profile. In Fig. 4, swath width was 20 km for each profile (indicated in Fig. 4a with triple lines). Major changes in lithology are marked above each

**Fig. 4** Results of random forest modelling. **a** Final $^{87}Sr/^{86}Sr$ isoscape map produced by the random forest ▶ method of Bataille et al. (2018), using the entire dataset of new $^{87}Sr/^{86}Sr$ data together with 23 auxiliary variables. For comparison, the data points are colour-coded with the same scale. Each set of 3 parallel lines represents the position and width of one swath profile. **b** Swath profiles across the $^{87}Sr/^{86}Sr$ isoscape map. Main lithology and rock age are assigned along the profiles as coloured bars. Swath width is 20 km in each profile. The black line represents the mean, and the red lines are the maximum and minimum $^{87}Sr/^{86}Sr$ at each point along the profile lines. Physiographic regions (Fig. 1c) are labelled. Abbreviations are: SHB—Subhercynian Basin, HM—Harz Mountains, TB—Thuringian Basin, SGB—South German Basin, LB—Lusatian Block, EG—Eger Graben, FB–Fichtelgebirge and Erzgebirge, TFB—Thuringian Forest Basin, TFSB—Thuringian-Franconian Slate Belt, NGB—North German Basin, CB—Chemnitz Basin, SGM—Saxon Granulite Mountains, NSVC—North Saxon Volcanic Complex, BCB—Bohemian Cretaceous Basin
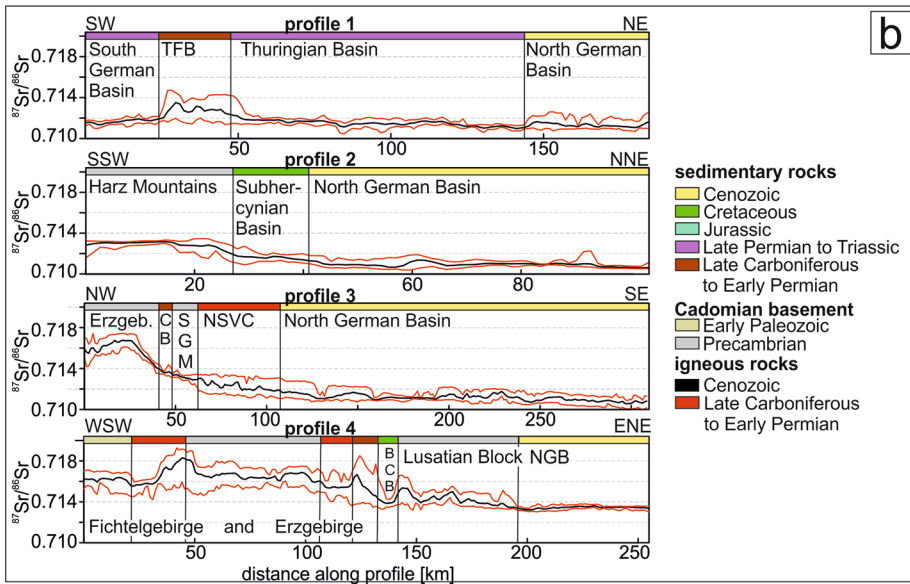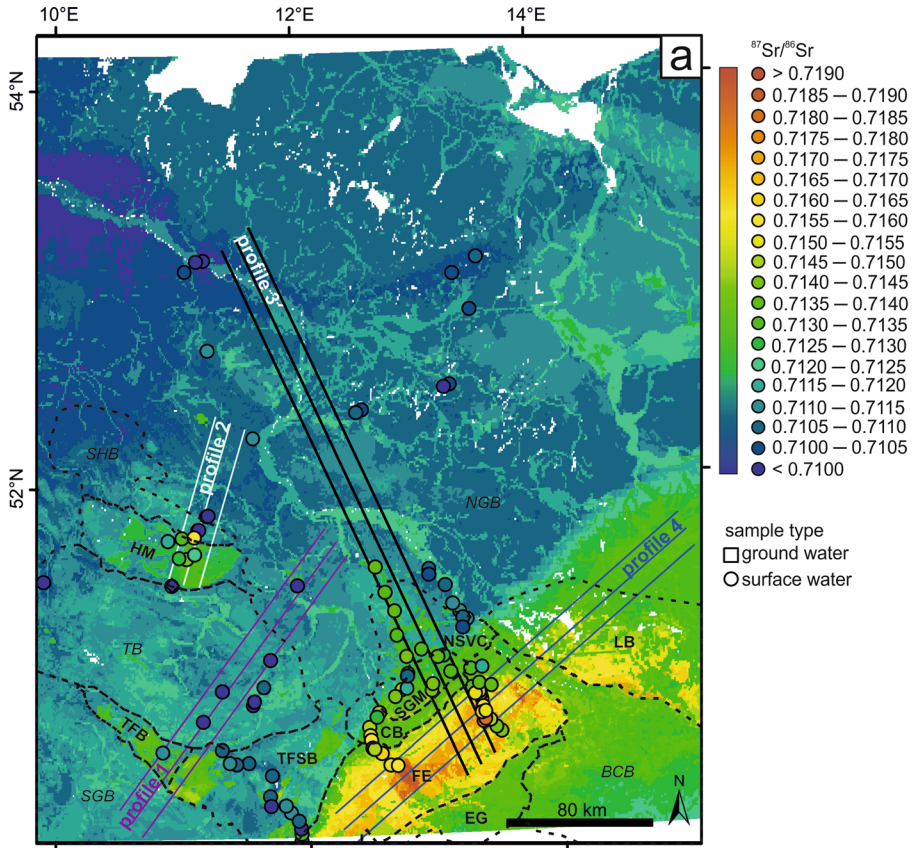
profile. The combination of mean $^{87}Sr/^{86}Sr$ ratios with lithological changes visualizes the relationship between lithology and the strontium isotopic composition of water. Additionally, minimum and maximum $^{87}Sr/^{86}Sr$ ratios along the profiles allow assessing the variability of the strontium isotopic composition within each geologically coherent region.

## 4  Discussion

### 4.1  Water $^{87}Sr/^{86}Sr$ Ratios of Central and NE Germany

#### 4.1.1  Comparison of the $^{87}Sr/^{86}Sr$ Ratios of Stream Water and Groundwater

From the Freiberger Mulde catchment data, we aimed to define the type of water samples that optimally reflects the local $^{87}Sr/^{86}Sr$ ratio. For this, we compared the water of the Freiberger Mulde river with smaller tributaries and with groundwater. The median values of all three groups are similar (ca. 0.1 mg/l Sr, $^{87}Sr/^{86}Sr \sim 0.715$, Fig. 2b, c).

However, the variability of $^{87}Sr/^{86}Sr$ ratios and strontium concentrations in the Freiberger Mulde catchment is higher for smaller tributaries than for the main stream and highest for groundwater samples (Fig. 2b, c). In comparison with stream water, groundwater is probably much more influenced by very local geologic phenomena like faults, ore lodes, volcanic dykes, and anthropogenic pollution such as fertilizers (Böhlke and Horan 2000; Thomsen and Andreasen 2019), mine waters (Zieliński et al. 2018), or other groundwater contamination (Nigro et al. 2017). Still, in contrast to completely stationary proxies like plant leaves, roots, or soils, a slightly reduced variability in groundwater can be assumed due to some horizontal and vertical groundwater flow (Ladegaard-Pedersen et al. 2020).

These differences in variability between small streams, larger streams, and groundwater are probably related to mixing processes in stream water. Mixing processes can be recognized in mixing diagrams, where two end-members define a line in an $^{87}Sr/^{86}Sr$ vs. 1/Sr diagram and the mixed component will plot exactly on this line (e.g. Tichomirowa et al. 2010). However, in the Freiberger Mulde catchment area, a more complex mixing process is observed, because the mixing product (FM4 in Fig. 5a) is not situated on this straight line, so that one or more additional major sources contributed to the $^{87}Sr/^{86}Sr$ ratio of sampling point FM 4. The isotope ratio and Sr concentration of sampling points FM5 and FM6 should result from mixing between FM4- and TR3-waters. However, the mixing diagram reveals an additional input from sampling point TR4 (Fig. 5b). This discussion demonstrates that mixing and transport have a high impact on the Sr isotope ratio of stream water, so that each point in the stream network depends on all its upstream points (Brennan et al. 2016).

In difference, the groundwater $^{87}Sr/^{86}Sr$ ratios cannot be explained by simple mixing relationships. We found large differences (up to 0.004) between the predicted Sr isotope ratios from the stream network model and the measured $^{87}Sr/^{86}Sr$ ratios in groundwater near the streams. This also emphasizes the high influence of local factors on groundwater.

Based on these results, we decided to concentrate on river water instead of groundwater to constrain the local $^{87}Sr/^{86}Sr$ ratios of various physiographic regions for Central and North Germany. We avoided groundwater sampling, because very local geologic phenomena and anthropogenic factors should not be included in a local $^{87}Sr/^{86}Sr$ signature.
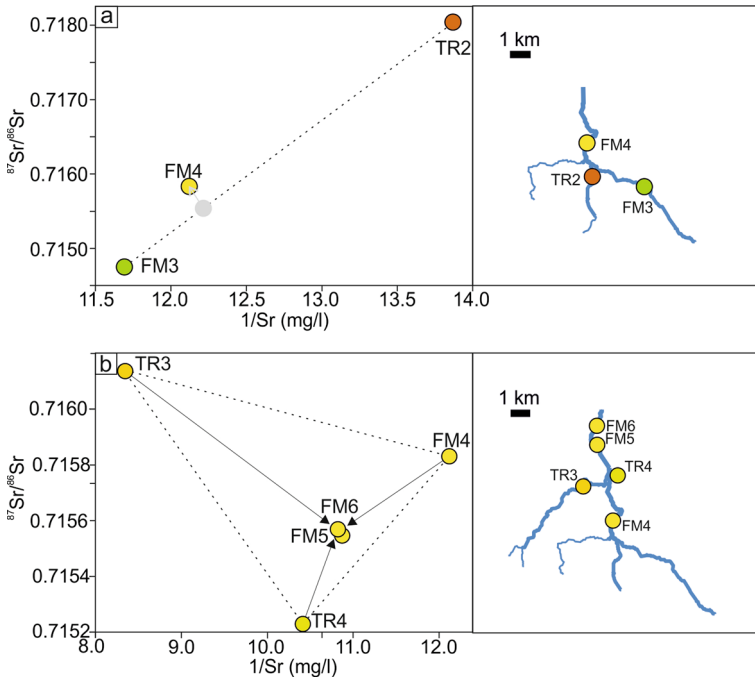
**Fig. 5** Mixing relationships in the Freiberger Mulde catchment. Mixing relationships are shown in the left column. The right column represents the position of the samples within the stream network a) Mixing line of the two end-members FM3 and TR2. Mixing products are situated along the connecting line. The position of a theoretical mixing product and the deviation of sample FM4 from this position are shown as a grey point and arrow, respectively. b) Mixing triangle of the three end-members FM4, TR3, and TR4. Samples FM5 and FM6 are situated inside the triangle and are thus potential mixing products of these end-members

Furthermore, the high variability of groundwater $^{87}$Sr/$^{86}$Sr ratios would require a much higher amount of samples to define a robust mean value for a region. Instead, we sampled large streams to obtain averaged values for larger regions, and smaller streams to represent smaller-scale variations.

### 4.1.2 Dependency of Stream Water $^{87}$Sr/$^{86}$Sr on Lithology and Rock Age

As expected, we observe clear differences between stream water that flows on sedimentary basins and water that flows in mountainous regions. The dependency of $^{87}$Sr/$^{86}$Sr on lithology and rock age is illustrated in swath profiles that include both mountainous regions and sedimentary basins (Fig. 4b). Higher $^{87}$Sr/$^{86}$Sr ratios were determined in the mountainous regions of the Erzgebirge/Fichtelgebirge (0.71216–0.72313), the Harz Mountains (0.70998–0.71869), the Thuringian-Franconian Slate Belt (0.70910–0.71414), the Thuringian Forest Basin (0.71128), the Chemnitz Basin (0.71283–0.71579), the Granulite Mountains (0.71150–0.71455), and the North Saxon Volcanic complex (0.71326–0.71411). All these regions are characterized by Precambrian and Palaeozoic granitic gneisses, granites, rhyolites and clastic sediments (Table 4). In contrast, water from sedimentary basins revealed lower values. Thereby, basins filled with Cenozoic sediments (North German Basin: 0.70888–0.71149),

**Table 4** Summary of published, measured, and modelled $^{87}$Sr/$^{86}$Sr ratios in physiographic regions of Central and NE Germany (defined in Fig. 1)

| Physiographic region | $^{87}$Sr/$^{86}$Sr measured | $^{87}$Sr/$^{86}$Sr published | $^{87}$Sr/$^{86}$Sr from modelling | prevalent lithologies |
|---|---|---|---|---|
| Thuringian Forest Basin | 0.71128 (n=1) | 1: 0.70804 (n=1) | Mean=0.71285 Min=0.71105 Max=0.71414 SD=0.00104 | dominantly Late Carboniferous to Early Permian rhyolitic volcanic rocks, interbedded with strata of continental conglomerate and sandstone (Lützner et al. 2012) |
| Thuringian Basin | 0.70794–0.71098 (n=16) | 3: 0.70801–0.71178 (n=18) 1: 0.7104–0.71087 (n=3) | Mean=0.71152 Min=0.70953 Max=0.71305 SD=0.00043 | Triassic sediments: interbedded strata of marine deposits (carbonate, salt, gypsum, and clastic sediment) and terrestrial (clastic) sediment (Hoppe and Seidel 1971) |
| South German Basin | 0.71190 (n=1) | 1: 0.70837–0.71011 (n=9) | Mean=0.71144 Min=0.71024 Max=0.71272 SD=0.00036 | Triassic sediments: interbedded strata of marine deposits (carbonate, salt, gypsum and clastic sediment) and terrestrial (clastic) sediment (Doben et al. 1996) |
| Thuringian-Franconian Slate Belt | 0.70910–0.714414 (n=17) | | Mean=0.71199 Min=0.71019 Max=0.71472 SD=0.00101 | Precambrian to Palaeozoic greywacke, shale, limestone, and quartzite, mafic volcanic rocks at the transition to the Fichtelgebirge, metamorphically overprinted in the Late Carboniferous (BGR, 2014) |
| Erzgebirge and Fichtelgebirge | 0.71216–0.72313, outlier: 0.74363 (n=37) | 1: 0.71840–0.72900 (n=2) 2: 0.71216–0.71748 (n=8) | Mean=0.71601 Min=0.71274 Max=0.71949 SD=0.00115 | Precambrian to Palaeozoic clastic sedimentary and igneous rocks, juxtaposed marine clastic sediments, metamorphosed to gneiss, eclogite, phyllite and micaschist in the Late Carboniferous (Hoth et al. 1995; Mingram 1998); occasionally Late Carboniferous to Early Permian granite and rhyolite (Hoth et al. 1995; Förster et al. 1999; Hoffmann et al. 2013) |

**Table 4** (continued)

| Physiographic region | $^{87}Sr/^{86}Sr$ measured | $^{87}Sr/^{86}Sr$ published | $^{87}Sr/^{86}Sr$ from modelling | prevalent lithologies |
|---|---|---|---|---|
| Lusatian Block | None | 1: 0.71282–0.71435 (n=2) | Mean=0.71418 Min=0.71263 Max=0.71718 SD=0.00098 | Cadomian igneous rocks and Cambrian to Late Visean greywacke, largely unmetamorphosed (Kozdrój et al. 2001; Kroner et al. 2007); partial coverage with Cenozoic sandstone and siltstone, and intrusion of Cenozoic mafic volcanics (Malkowsky 1987) |
| Eger Graben | None | 1: 0.70403–0.70823, outlier: 0.72038 (n=3) | Mean=0.71354 Min=0.71237 Max=0.71668 SD=0.00069 | mainly fluviatile Cenozoic sandstone and siltstone that comprises lignite, juxtaposed with Cenozoic mafic volcanic rocks (Rajchl et al. 2008) |
| Chemnitz Basin | 0.71283–0.715579 (n=5) | 1: 0.71297–0.71247 (n=2) | Mean=0.71332 Min=0.71180 Max=0.71415 SD=0.00061 | dominantly Late Carboniferous to Early Permian continental conglomerate and sandstone, interbedded with rhyolitic volcanic rocks (Schneider et al. 2012) |
| Saxon Granulite Mountains | 0.71150–0.71455 (n=10) | None | Mean=0.71321 Min=0.71273 Max=0.71416 SD=0.00027 | granulite, surrounded by an outer slate mantle of Cambrian phyllite, quartzite, greywacke, and shale, metamorphic overprint in the Late Carboniferous, outward decreasing metamorphic grade (Kroner 1995) |
| North Saxon Volcanic Complex | 0.71326–0.71411 (n=6) | None | Mean=0.71226 Min=0.71097 Max=0.71351 SD=0.00080 | Late Carboniferous to Early Permian volcanic rocks (Hübner et al. 2021) |

**Table 4** (continued)

| Physiographic region | $^{87}Sr/^{86}Sr$ measured | $^{87}Sr/^{86}Sr$ published | $^{87}Sr/^{86}Sr$ from modelling | prevalent lithologies |
|---|---|---|---|---|
| Harz Mountains | 0.70998–0.71869 (n = 14) | 1: 0.70736–0.70759 (n = 2) | Mean = 0.71222 Min = 0.71058 Max = 0.71341 SD = 0.00074 | Precambrian to Early Paleozoic marine sediment, weak metamorphic overprint to greywacke, and phyllite in the Late Carboniferous (Spiess et al., 1998, Martiklos 2002); occasionally Late Carboniferous to Early Permian granites and rhyolites, (Zech et al. 2010) |
| Subhercynian Basin | 0.70904–0.71079; outlier: 0.71586 (n = 5) | 1: 0.70879–0.70887 (n = 2) | Mean = 0.71097 Min = 0.71017 Max = 0.71210 SD = 0.00038 | Early Cretaceous marlstone and sandstone and Late Cretaceous siliciclastic shallow marine and continental sandstone, Jurassic marine marlstone, limestone, and sandstone, (Voigt 2004) |
| North German Basin | 0.70888–0.71149, outliers: 0.71425, 0.71468, 0.71528 (n = 27) | 1: 0.70928–0.71031 (n = 18) | Mean = 0.71110 Min = 0.70968 Max = 0.71409 SD = 0.00067 | Uniform coverage of Cenozoic glacial till, clastic sandstone and siltstone, and small occurrences of peat (Hinze 1986; Lippstreu et al. 1997; Krienke 2003) |
| Bohemian Cretaceous Basin | None | 1: 0.72038 (n = 1) | Mean = 0.71088 Min = 0.71021 Max = 0.71114 SD = 0.00040 | Early Cretaceous marlstone and sandstone and Late Cretaceous siliciclastic shallow marine and continental sandstone (Mrázová et al. 2020); partly covered by Cenozoic sediments, occurrences of Cenozoic mafic volcanic rocks (Ulrych et al. 2011) |

n = number of samples, data sources: 1: Voerkelius et al. (2010), 2: Tichomirowa et al. (2010), 3: Maurer et al. (2012), abbreviations are: Min - minimum, Max - maximum, SD - standard deviation

or with Mesozoic sediments (Thuringian basin: 0.70794–0.71098, South German Basin: 0.71190, Subhercynian basin: 0.70904–0.71079) cannot be discriminated from each other by their $^{87}Sr/^{86}Sr$ ratios. Inside one lithologically uniform (physiographic) region, mean $^{87}Sr/^{86}Sr$ ratios appear to be rather uniform, whereas sharp changes can be observed near the boundaries between mountainous regions and sedimentary basins.

### 4.1.3 Changes of Stream Water $^{87}Sr/^{86}Sr$ Ratios Across Geological Boundaries

Due to mixing and transport processes in the stream network, the $^{87}Sr/^{86}Sr$ ratio at any point along a stream represents a mixture of the $^{87}Sr/^{86}Sr$ ratios of this point´s entire catchment (Brennan et al. 2016). Thus, stream water $^{87}Sr/^{86}Sr$ ratios do not necessarily represent the local biologically available strontium, but might be influenced by distant lithologies. Since we used stream water $^{87}Sr/^{86}Sr$ data to produce our final isoscape map, this influence of transport and mixing has to be analysed. In the geologically complex area of Central and NE Germany, it is important to know how far $^{87}Sr/^{86}Sr$ ratios are transported from mountainous regions into sedimentary basins.

Our data and the stream network model of the Freiberger Mulde catchment (Fig. 2a) illustrate that the $^{87}Sr/^{86}Sr$ ratio along streams is strongly influenced by the lithology and rock age, but does not change abruptly when the stream enters or crosses a different rock type. Strong changes are typically observed at confluences of two or more streams of similar size when the influencing catchment increases suddenly (Fig. 2a). From the upper part of the Freiberger Mulde (samples FM1, FM2, and FM3 in Fig. 2a), we conclude that water draining grey gneisses has an $^{87}Sr/^{86}Sr$ ratio of 0.7141–0.7148. Frequent occurrences of rhyolitic dykes cut the grey gneisses. These dykes are expected to increase the $^{87}Sr/^{86}Sr$ ratio, but do not show a significant impact on the $^{87}Sr/^{86}Sr$ ratios of the stream water. However, an increase of $^{87}Sr/^{86}Sr$ ratios is observed in the SW of the Freiberger Mulde as an effect of tributary TR2 draining outcrops of red gneisses (Fig. 2a). The Freiberger Mulde returns to the previous values (typical for grey gneisses) after ca. 20 km along stream (after passing sampling point FM 10; Fig. 2a).

In agreement with our observations from the Freiberger Mulde catchment, high $^{87}Sr/^{86}Sr$ ratios are transported into the sedimentary basins for not more than a few tens of kilometres in the swath profiles of the final isoscape map (Fig. 4a).

For the area of Central and NE Germany, we conclude that river water $^{87}Sr/^{86}Sr$ is strongly influenced by mixing and transport processes along stream, but is nevertheless a suitable proxy for the local biologically available strontium isotopic composition. Although it might change dramatically at confluences, it adapts its $^{87}Sr/^{87}Sr$ ratio to the major geology within a few tens of kilometres along stream. However, we cannot assess this effect for larger streams and their tributaries.

## 4.2 Accuracy of the Spatial Stream Network Model of the Freiberger Mulde Catchment

We assessed the accuracy of the stream network model by comparing the mean of the closest upstream- and downstream $^{87}Sr/^{86}Sr$ predictions with each measured ratio. Deviations of the modelled from the measured ratios are $\leq 0.0005$ and typically below 0.0002.

### 4.3 Performance of the Machine Learning Model

#### 4.3.1 Auxiliary Variable Impact

A plot of the relative importance of auxiliary variables (Fig. 3) shows that the process-based bedrock model of Bataille et al. (2018) has the largest influence on our model and provides three of the most important variables (the first and third quartiles and mean).

In addition to the bedrock model, we found that the sea salt wet and dry deposition has a major influence on our model (Fig. 3). Central and NE Germany is bordered to approximately ¼ by the coastline to the Baltic Sea. It has a maximum distance from the coast of ca. 430 km. It has been shown that sea salt deposition (sea spray) plays a major role at localities as far as 300 km inland from the coast (Gustafsson and Franzén, 2000; Ladegaard-Pedersen et al. 2020). Possibly, this explains the relatively high impact on the strontium isotopic composition of Central and NE Germany. On the other hand, a crucial contribution of sea salt deposition to Denmark (Frei and Frei 2011) and to Poland (Zieliński et al. 2021), which are located in similar geographic and climatic conditions, was not observed. Thus, it is possible that the correlation between sea salt deposition and surface water $^{87}Sr/^{86}Sr$ that was found during random forest modelling, was spurious. Any other parameter that correlates with the distance from the sea could have caused a spurious correlation with sea salt deposition. One possible variable might be the thickness of sediments on the Pre-Permian crystalline basement. These sediments were deposited within the Southern Permian Basin. The southern rim of the Basin was situated close to the recent Fichtelgebirge/Erzgebirge, and the depocenter with the highest sediment thicknesses was located close to the coast line of the recent Baltic Sea (Ziegler 1990) so that the sediment thickness decreased towards South.

The Bouguer anomaly is another auxiliary variable with a high impact. Probably, there is no direct correlation between $^{87}Sr/^{86}Sr$ and the Bouguer anomaly. This variable depends, among other things, on the density and thus on the lithology of bedrock. An influence of deep subsurface rocks on the strontium isotopic composition of stream waters and groundwaters can be excluded. Nevertheless, a comparison of the density of surface bedrock and Bouguer anomaly shows good agreement for the Bohemian Massif (Meurers and Steinhauser 1990). Therefore, the Bouguer anomaly is probably a proxy for the surface lithology, which has an undisputable influence on the strontium isotopic composition (e.g. Beard and Johnson 2000; Bentley 2006; Voerkelius et al. 2010; Bataille et al. 2018).

Another important auxiliary variable was dust flux and dust sources, combined in a single variable (r.dust). The relationship between dust and strontium isotopic composition is complex and related to the $^{87}Sr/^{86}Sr$ of the provenance region(s) of the dust (Bataille et al. 2020). Especially in regions with slowly weathering rock types, like crystalline felsic rocks in the mountainous regions of Central and NE Germany (Fig. 1a), the influence of exogenous material might be significant. The impact of evapotranspiration (r.pet) on biologically available $^{87}Sr/^{86}Sr$ ratios is probably connected to dust and sea salt deposition, since it might control the relative contributions of bedrock-derived strontium versus aerosol- or dust-derived strontium (Bataille et al. 2018).

A potential impact of fertilizers (r.fert) on the $^{87}Sr/^{86}Sr$ ratios is typically observed in regions with a high percentage of agricultural land (e.g. Böhlke and Horan 2000; Thomsen and Andreasen 2019). The contribution of agricultural runoff in stream water has been estimated to be as high as 40% in the Karup river (Denmark, Thomsen and Andreasen 2019), and the fraction of agricultural strontium in the Oder river (Poland) has been estimated to

be around 50% (Zieliński et al. 2018). We assume that the amount of fertilizer has a comparably low impact on our model, because its IncNodePurity is lower than that of 6 other variables (Fig. 3).

In summary, from the auxiliary variable importance plot (Fig. 3), three sources can be identified that mainly contribute to the $^{87}$Sr/$^{86}$Sr ratio of bioavailable strontium in Central and NE Germany. These are: (1) rock-type related parameters like the bedrock lithology and rock age (in form of the bedrock model of Bataille et al. 2018) and the Bouguer anomaly (2) transport from external sources, including sea salt wet and dry deposition and dust input, and (3) anthropogenic influences (e.g. fertilizers).

### 4.3.2  Estimates for the Accuracy of Our Isoscape Map

The accuracy of our final isoscape map can be estimated through a comparison of measured and modelled data. The training and the testing datasets show a high correlation between the modelled and the measured values (Fig. 6a), suggesting a high accuracy of the modelled data. The regression line is close to, but not identical to the 1:1 line, suggesting a slight overestimation of the lowest and a very slight underestimation of the highest $^{87}$Sr/$^{86}$Sr ratios in the training data. The testing data fit better to the 1:1 line, but several single analyses and the lowest data (measured ratios < 0.711) deviate even more from this line (Fig. 6b).

Another way to quantify the accuracy of the model is the computation of its RSME (root mean square error, Bataille et al. 2018). In our case, the RSME is 0.0015. This is significantly lower than the RSME reported by Bataille et al. (2018) for their strontium isoscape of Central Europe (0.0023). A lower RSME indicates a better fit between modelled and measured data.

For each physiographic region, the accuracy of the final isoscape map can be assessed by the direct comparison between modelled and measured $^{87}$Sr/$^{86}$Sr ranges. To do this, we extracted the range of $^{87}$Sr/$^{86}$Sr ratios for each of the defined physiographic regions (Fig. 1c) from our data and the final isoscape map. Since the $^{87}$Sr/$^{86}$Sr ratios are variable at a certain distance around the boundaries between regions (Fig. 4b), we sampled the range
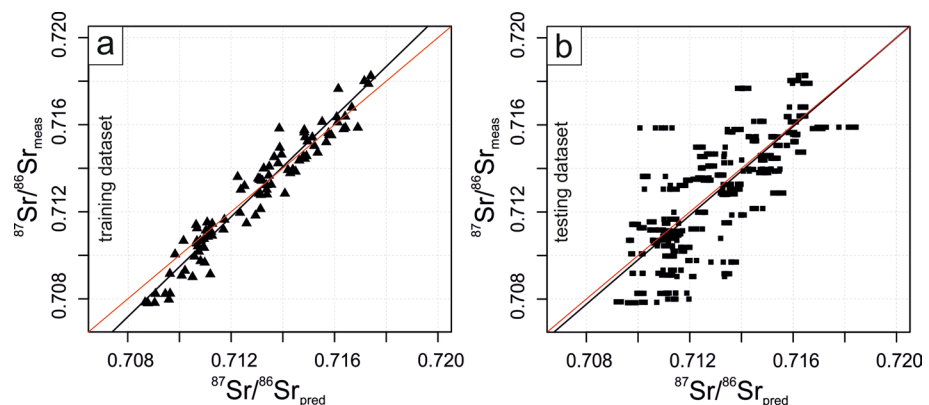


**Fig. 6** Measured vs. predicted $^{87}$Sr/$^{86}$Sr ratios for random forest modelling. To assess the accuracy and precision of the model, the dataset was randomly split into a training subset (80% of the entire dataset) and a testing holdout subset for validation (20% of the total dataset). Regression lines are shown in black, 1:1 lines are shown in red. a) Comparison of predicted values with the training dataset. b) Comparison of predicted values with the testing dataset (tenfold cross-validation)
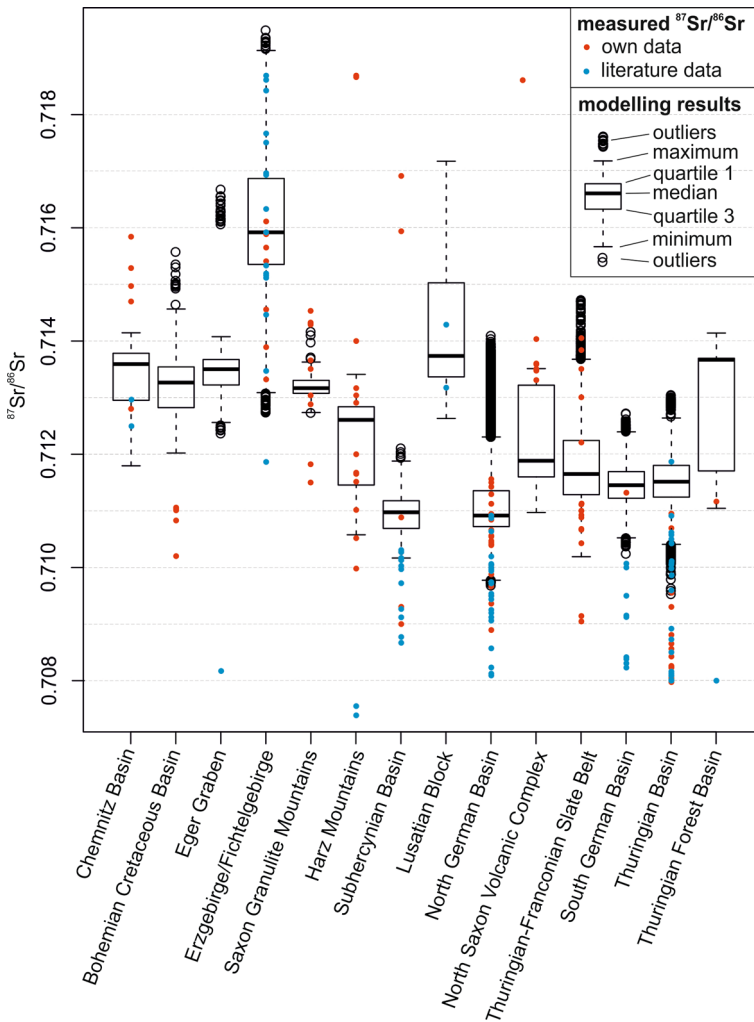
**Fig. 7** Box plots of the $^{87}$Sr/$^{86}$Sr data of the modelled isoscape map, grouped by physiographic regions (Fig. 1c). For comparison, data from this study (red) and literature data from water samples of Central and NE Germany (blue, Voerkelius et al. 2010; Tichomirowa et al. 2010; Maurer et al. 2012) were plotted for each region

of ratios from the interior of each region. For this, we applied a buffer distance of 5 km from the region boundaries. The data are presented as box plots in Fig. 7. In Table 4, we compile the mean, minimum, maximum and standard deviations of our model for each physiographic region, compare these data with new and published $^{87}$Sr/$^{86}$Sr ratios, and give a brief summary of the geological setting for each region. While most regions reveal a unimodal distribution around a mean value, others display a bimodal distribution of the $^{87}$Sr/$^{86}$Sr (Fig. 7, e.g. the North German Basin, and the Thuringian-Franconian Slate belt). In boxplots, this results in a high number of outliers towards higher or lower values.

For our isoscape map, we can show that the mean (Table 4) and median (Fig. 7) modelled value is within the measured data range in most regions. The best fit between the values of the model and measured $^{87}Sr/^{86}Sr$ ratios, both in absolute data and in data variability, is reached for the Erzgebirge/Fichtelgebirge region, the Saxon Granulite Mountains, the Harz Mountains, and the Thuringian Franconian Slate Belt (Fig. 7, Table 4). Only in the Eger Graben, the Bohemian Cretaceous Basin, the Thuringian Forest Basins and the Subhercynian Basin, the modelled mean and median $^{87}Sr/^{86}Sr$ are outside the range of measured data (Table 4, Fig. 7). We assume that the extremely low number of measured data (0–4 observations for the above mentioned regions) is the reason for this. The absolute deviation of the mean modelled from measured data is as high as around 0.005 in the Eger Graben (no observations), 0.002 in the Bohemian Cretaceous Basin (4 observations), and 0.0016 in the Thuringian Forest Basin (1 observation). We conclude that the accuracy of our model depends on the number of samples that were used for modelling.

In summary, the accuracy of our new isoscape map is generally strong, but our model seems to slightly overestimate $^{87}Sr/^{86}Sr$ ratios in several regions, especially in sedimentary basins with generally low $^{87}Sr/^{86}Sr$ ratios and a low sampling density, like the N German Basin, the Subhercynian Basin, the Thuringian Basin, and the Bohemian Cretaceous Basin (Fig. 7).

### 4.4 Comparison with Published $^{87}Sr/^{86}Sr$ Data and Isoscape Maps of Central and NE Germany

We present the first $^{87}Sr/^{86}Sr$ isoscape map that covers entire Central and NE Germany with a very high resolution and accuracy, both in sampling and modelling (Fig. 7, Table 4). Some previously published datasets (Voerkelius et al. 2010; Tichomirowa et al. 2010; Maurer et al. 2012) and isoscape maps (Hoogewerff et al. 2019; Bataille et al. 2018, 2020) include at least parts of Central and NE Germany and can be compared to our results.

Similar to our data and model, Voerkelius et al. (2010) and Tichomirowa et al. (2010) found high $^{87}Sr/^{86}Sr$ ratios in the water of the mountainous regions of the Erzgebirge/Fichtelgebirge and the Chemnitz Basin (Table 4). Our new data from the Freiberger Mulde and its tributaries are within the range of published $^{87}Sr/^{86}Sr$ ratios from this catchment (Tichomirowa et al. 2010). Additionally, our new data from some sedimentary basins (the Thuringian Basin, the Subhercynian Basin, and the North German Basin) are within the previously published range of data (Table 4; Voerkelius et al. 2010; Maurer et al. 2012). In contrast to this, the previously published $^{87}Sr/^{86}Sr$ ratios of the Harz Mountains and the Thuringian Forest Basin (Voerkelius et al. 2010) differ significantly from our new data, which are much higher (Table 4). The reason for such differences might be a too small number of published data from the Harz Mountains and the Thuringian Forest Basin, so that a statistically robust data range could not be defined. Our sampling campaign solved this problem for the Harz Mountains, but not for the Thuringian Forest Basin, where we added only one single measurement to the database.

Our new data reveal a significant difference between $^{87}Sr/^{86}Sr$ ratios in mountainous regions (Erzgebirge/Fichtelgebirge, Harz Mountains) and sedimentary basins (North German Basin, Thuringian Basin). We conclude that isoscape maps with uniform and low $^{87}Sr/^{86}Sr$ ratios for entire Central and NE Germany (Hoogewerff et al. 2019; Bataille et al. 2020) are not correct. This might be attributed to an insufficient resolution of the maps (Bataille et al. 2020) or an insufficient sampling density (Hoogewerff et al. 2019).

Furthermore, these isoscape maps are not based on water samples, but mainly on soil lea-chates (Hoogewerff et al. 2019; Bataille et al. 2020). This might induce a small difference in $^{87}Sr/^{86}Sr$, but a generally good correlation between the $^{87}Sr/^{86}Sr$ ratios in water and soil leachates has been demonstrated (Ladegaard-Pedersen et al. 2020). Thus, the difference of $^{87}Sr/^{86}Sr$ ranges between mountainous regions and sedimentary basins should be recogniz-able from both materials.

The isoscape map of Western Europe of Bataille et al. (2018) shows strong variability, with higher $^{87}Sr/^{86}Sr$ ratios in mountainous regions and lower ratios in sedimentary basins. But here, these differences are obviously not based on measured data, which were sampled in the Thuringian Basin only (Bataille et al. 2018).

As outlined by Bataille et al. (2020), a robust estimate can only be expected in data-rich areas and if sampling covers all geological variations. This is in accord with our observa-tion and a direct comparison of the isoscape map of Bataille et al. (2018) with our new isoscape map can reveal the strengths and weaknesses of both models (Fig. 8). Apparently, the isoscape map of Bataille et al. (2018) underestimates the $^{87}Sr/^{86}Sr$ ratios in moun-tainous regions like the Erzgebirge and the Harz mountains (Fig. 8a, c). Probably, this is because the map was produced without measured data from these regions. In contrast, the modelled $^{87}Sr/^{86}Sr$ ratios of the Thuringian Basin, which was part of these authors' sam-pling approach, are well reproduced (Fig. 8a). In difference, our new isoscape map slightly overestimates the $^{87}Sr/^{86}Sr$ ratio in the Thuringian Basin (Fig. 8b), although our 16 new data from the Thuringian Basin do not differ from the dataset used by Bataille et al (2018; Fig. 7).

For our modelling, we used the approach of Bataille et al. (2018) with almost identical auxiliary variables. Thus, the distribution of samples must be the reason for differences in the isoscape maps. Our samples were mainly derived from mountainous regions (Fig. 1c). Consequently, most of the variability in our dataset is found in these regions. Since the machine learning model aims to explain as much as possible of the variability of a dataset, this selective sampling approach optimized our model for mountainous regions. This is
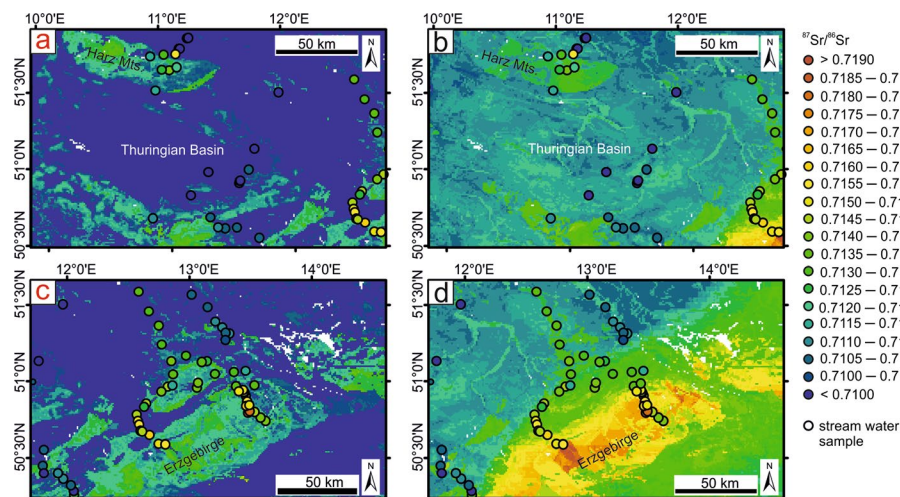


**Fig. 8** Comparison of the published strontium isoscape map of Bataille et al. (2018, left column) with our new isoscape map (right column). a, b) Thuringian Basin with Harz mountains. c, d) Erzgebirge/Fichtelge-birge and foreland. The colour scale of all four maps is identical

different to the observations of Bataille et al. (2020) and Brennan et al. (2016), who stated that the modelling approach is not adequate for geologically complex areas. Our study demonstrates that geologically complex areas can be modelled correctly if the sampling density is high enough. Nevertheless, a relative uniform sampling approach is necessary to maintain a similar grade of accuracy for an entire isoscape map.

# 5 Conclusions

From 119 new stream water and groundwater $^{87}Sr/^{86}Sr$ data, we modelled a strontium isoscape map of Central and NE Germany. For this, we used the machine learning method of Bataille et al. (2018) with 23 auxiliary variables.

To support meaningful provenance interpretations in archaeology and animal migration studies, we subdivided the area of Central and NE Germany into 14 geologically coherent regions. We focussed our sampling on the mountainous regions of the Erzgebirge/Fichtelgebirge and the Harz mountains, which were not well represented by measured $^{87}Sr/^{86}Sr$ values in previously published isoscape maps (Bataille et al. 2018, 2020; Hoogewerff et al. 2019) and regional studies (Voerkelius et al. 2010).

In our new data and model, these mountainous regions reveal significantly increased $^{87}Sr/^{86}Sr$ ratios in comparison with adjacent sedimentary basins like the Thuringian Basin, the North German Basin, or the Subhercynian Basin. The comparison with existing data and isoscape maps of Central and NE Germany demonstrates that our new isoscape map is the first that resembles stream water $^{87}Sr/^{86}Sr$ ratios in mountainous regions with very high accuracy.

Our results demonstrate the need for an increased sampling density in geologically complex areas to cover all possible $^{87}Sr/^{86}Sr$ ranges. This is particularly important for studies of migration over short distances, in which the origin and destination of an individual might have similar, but not identical $^{87}Sr/^{86}Sr$. For such studies, isoscape maps are not sufficient to define possible provenance regions, because they do not present uncertainties and ranges of measured data. Instead, each geologically uniform region should be characterized precisely from measured data. Here, we provide a database of Central and NE Germany, in which we present the number and the range of measured data together with mean, minimum and maximum values, and standard deviations of the final isoscape map (Table 4). Such statistical information can be used directly in archaeology and animal migration studies.

# Declarations

**Conflict of interest** The authors have no competing interests to declare that are relevant to the content of this article.

**Open Access** This article is licensed under a Creative Commons Attribution 4.0 International License, which permits use, sharing, adaptation, distribution and reproduction in any medium or format, as long as you give appropriate credit to the original author(s) and the source, provide a link to the Creative Commons licence, and indicate if changes were made. The images or other third party material in this article are included in the article's Creative Commons licence, unless indicated otherwise in a credit line to the material. If material is not included in the article's Creative Commons licence and your intended use is not permitted by statutory regulation or exceeds the permitted use, you will need to obtain permission directly from the copyright holder. To view a copy of this licence, visit http://creativecommons.org/licenses/by/4.0/.

# References

Balmino G, Vales N, Bonvalot S, Briais A (2012) Spherical harmonic modelling to ultra-high degree of Bouguer and isostatic anomalies. J Geod 86:499–520

Bataille CP, Brennan SR, Hartmann J, Moosdorf N, Wooller MJ, Bowen GJ (2014) A geostatistical framework for predicting variability in strontium concentrations and isotope ratios in Alaskan rivers. Chem Geol 389:1–15

Bataille CP, von Holstein ICC, Laffoon JE, Willmes M, Liu XM, Davies GR (2018) A bioavailable strontium isoscape for Western Europe: a machine learning approach. PLoS ONE 13:1–27

Bataille CP, Crowley BE, Wooller MJ, Bowen GJ (2020) Advances in global bioavailable strontium isoscapes. Palaeogeograph Palaeoclimatol Palaeoecol 555:109849

Bataille CP, Jaouen K, Milano S, Trot M, Steinbrenner S, Crubézy É, Colleter R (2021) Triple sulfur-oxygen-strontium isotopes probabilistic geographic assignment of archaeological remains using a novel sulfur isoscape of western Europe. PLoS ONE 16(5):e0250383

Beard BL, Johnson CM (2000) Strontium Isotope Composition of Skeletal Material can determine the birth place and geographic mobility of humans and animals. J Forensic Sci 45(5):1049–1061

Bentley RA (2006) Strontium isotopes from the earth to the archaeological skeleton: a review. J Archaeol Method Theory 13(3):135–187

Böhlke JK, Horan M (2000) Strontium isotope geochemistry of groundwaters and streams affected by agriculture Locust Grove, MD. Appl Geochem 15:599–609

Börker J, Hartmann J, Amann T, Romero-Mujalli G (2018) Terrestrial sediments of the earth: development of a global unconsolidated sediments map database (gum). Geochem Geophys Geosyst 19:997–1024

Brennan SR, Torgersen CE, Hollenbeck JP, Fernandez DP, Jensen CK, Schindler DE (2016) Dendritic network models: Improving isoscapes and quantifying influence of landscape and in-stream processes on strontium isotopes in rivers. Geophys Res Lett 43:5043–5051

Bundesanstalt für Geowissenschaften und Rohstoffe (BGR) (2014) Geological Map of Germany 1:1,000,000, (GK1000), Hannover

Charlier BL, Ginibre C, Morgan D, Nowell GM, Pearson DG, Davidson JP, Ottley CJ (2006) Methods for the microsampling and high-precision analysis of strontium and rubidium isotopes at single crystal scale for petrological and geochronological applications. Chem Geol 232(3–4):114–133

Conrad O, Bechtel B, Bock M, Dietrich H, Fischer E, Gerlitz L, Wehberg J, Wichmann V, Boehner J (2015) System for automated geoscientific analyses (SAGA) v. 2.1.4. Geosci Model Dev 8:1991–2007

Crowley BE, Miller JH, Bataille CP (2017) Strontium isotopes ($^{87}$Sr/$^{86}$Sr) in terrestrial ecological and palaeoecological research: empirical efforts and recent advantages in continental-scale models. Biol Rev 92:43–59

Doben K, Doppler G, Freudenberger W, Jerz H, Meyer RKF, Mielke H, Ott W-D, Rohrmüller J, Schmidt-Kaler H, Schwerd K, Unger HJ (1996) Geologische Karte von Bayern (4. Aufl.), Bayerisches Geologisches Landesamt, Augsburg

Faure G, Mensing M (2005) Isotopes: principles and applications, 3rd edn. Wily, New York, pp 412–446

Förster HJ, Tischendorf G, Trumbull RB, Gottesmann B (1999) Late-Collisional granites in the Variscan Erzgebirge, Germany. J Petrol 40:1613–1645

Frei KM, Frei R (2011) The geographic distribution of strontium isotopes in Danish surface waters—a base for provenance studies in archaeology, hydrology and agriculture. Appl Geochem 26:326–340

Frei KM, Villa C, Jørkov ML, Allentoft ME, Kaul F, Ethelberg P, Reiter SS, Wilson AS, Olsen J, Lynnerup N, Willerslev E, Kristiansen K, Frei R (2017) A matter of months: high precision migration chronology of a Bronze Age female. PLoS ONE 12:e0178834

Grimstead DN, Nugent S, Whipple J (2017) Why standardization of strontium isotope baseline environmental data is needed and recommendations for methodology. Adv Archaeol Pract 5(2):184–195

Gustafsson MER, Franzén LG (2000) Inland transport of marine aerosols in southern Sweden. Atmos Environ 34:313–325

Hartmann J, Moosdorf N (2012) The new global lithological map database GLiM: a representation of rock properties at the Earth surface. Geochem Geophys Geosyst 13(12):12004

Hengl T, Mendes de Jesus J, Heuvelink GBM, Ruiperez Gonzalez M, Kilibarda M, Blagotić A, Shangguan W, Wright MN, Geng X, Bauer-Marschallinger B, Guevara MA, Vargas R, MacMillan RA, Batjes NH, Leenaars JGB, Ribeiro E, Wheeler I, Mantel S, Kempen B (2017) SoilGrids250m: global gridded soil information based on machine learning. PLoS ONE 12:e0169748

Hijmans RJ, Cameron SE, Parra JL, Jones PG, Jarvis A (2005) Very high resolution interpolated climate surfaces for global land areas. J Geod 25:1965–1978

Hinze C (1986) Geologische Übersichtskarte Von Niedersachsen: Mit Blattschnitt Der Geologischen Kartenwerke 1:200 000 Und 1:25 000, Niedersächs. Landesamt für Bodenforschung, Hannover

Hoffmann U, Breitkreuz C, Breiter K, Sergeev S, Stanek K, Tichomirowa M (2013) Carboniferous-Permian volcanic evolution in Central Europe—U/Pb ages of volcanic rocks in Saxony (Germany) and northern Bohemia (Czech Republic). Int J Earth Sci 102:73–99

Holt E, Evans JA, Madgwick R (2021) Strontium ($^{87}$Sr/$^{86}$Sr) mapping: a critical review of methods and approaches. Earth Sci Rev 216:103593

Hoogewerff J, Reimann C, Ueckermann H, Frei R, Frei KM, van Aswegen T, Striling C, Reid M, Clayton A, Ladenberger A, the GEMAS Project Team (2019) Bioavailable 87Sr/86Sr in European soils: a baseline for provenancing studies. Sci Total Environ 672:1033–1044

Hoppe W, Seidel G (1971) Geologische Karte Von Thüringen (Bezirke Erfurt, Gera, Suhl), Gotha

Hoth K, Wasternack J, Berger H-J, Breiter K, Mločoch B, Schovánek P (1995) Geologische Karte Erzgebirge/Vogtland 1:1000000, Sächsisches Landesamt für Umwelt und Geologie, Bereich Boden und Geologie

Hübner M, Breitkreuz C, Repstock A, Schulz B, Pietranik A, Lapp M, Heuer F (2021) Evolution of the Lower Permian Rochlitz volcanic system, Eastern Germany: reconstruction of an intra-continental supereruption. Int J Earth Sci 110:1995–2020

Isaak DJ, Peterson EE, Ver Hoef JM, Wenger SJ, Falke JA, Torgersen CE, Sowder C, Steel EA, Fortin M-J, Jordan CE, Ruesch AS, Som N, Monestiez P (2014) Applications of spatial statistical network models to stream data, WIREs Water. https://doi.org/10.1002/wat2.1023

Jarvis A, Reuter HI, Nelson AD, Guevara E (2008) Hole-filled SRTM for the globe Version 4, available from the CGIAR-CSI SRTM 90m Database. CGIAR CSI Consort. Spat. Information. http://srtm.csi.cgiar.org/

Kozdrój W, Krentz O, Opletal M (2001) Geological map and comments on the geological map Lausitz, Jizera, Karkonosze (without Cenozoic sediments) 1:100000. Państwowy Instytut Geologiczny, Warsaw

Krienke H-D (2003) Geologisches Landesamt Mecklenburg-Vorpommern. Geologische Karte von Mecklenburg-Vorpommern, Bundesrepublik, Deutschland

Kroner U (1995) Postkollisionale Extension am Nordrand der Böhmischen Masse: Die Exhumierung des Sächsischen Granulitgebirges, Freiberger Forschungshefte C; 457. Dt. Verl. für Grundstoffindustrie, Leipzig

Kroner U, Hahn T, Romer RL, Linnemann U (2007) The Variscan orogeny in the Saxo-Thuringian zone—Heterogenous overprint of Cadomian/Paleozoic Peri-Gondwana crust. Spec Paper Geol Soc Am 423:153–172

Kuhn M (2008) Building predictive models in R using the caret package. J Stat Softw 28:1–26

Ladegaard-Pedersen P, Achilleos M, Dörflinger G, Frei R, Kristiansen K, Frei KM (2020) A strontium isotope baseline of cyprus assessing the use of soil leachate, plants, groundwater and surface water as proxies for the local range of bioavailable strontium isotope composition. Sci Total Environ 708:134714

Lippstreu L, Hermsdorf N, Sonntag A, Brandenburg Landesamt für Geowissenschaften und Rohstoffe (1997) Geologische Übersichtskarte Des Landes Brandenburg. Landesvermessungsamt Brandenburg.

Lützner H, Andreas D, Schneider JW, Voigt S, Werneburg W (2012) Stefan und Rotliegend im Thüringer Wald und seiner Umgebung. In: Lützner H, Kowalczyk G (eds) Stratigraphie von Deutschland X. Rotliegend. Teil I: Innervariscische Becken. Schriftenreihe der Deutschen Gesellschaft für Geowissenschaften, Heft vol 61, pp 418–487.

Mahowald NM, Muhs DR, Levis S, Rasch PJ, Yoshioka M, Zender CS, Luo C (2018) Change in atmospheric mineral aerosols in response to climate: last glacial period, preindustrial, modern, and doubled carbon dioxide climates. Geochem J Geophys Res Atmos 111:D10202

Malkowsky M (1987) The mesozoic and tertiary basins of the Bohemian Massif and their evolution. Tectonophysics 137:31–42

Martiklos G (2002) Geologische Übersichtskarte Von Sachsen-Anhalt, Landesamt für Geologie und Bergwesen Halle/Saale

Maurer A-F, Galer SJG, Knipper C, Beierlein L, Nunn EBV, Peters D, Tütken T, Alt KW, Schöne BR (2012) Bioavailable $^{87}Sr/^{86}Sr$ in different environmental samples—effects of anthropogenic contamination and implications for isoscapes in past migration studies. Sci Total Environ 433:216–229

Meurers B, Steinhauser P (1990) Die Bouguer-Anomalie am Ostrand der Böhmischen Masse. Österr Beitr Met Geoph H3:13–23

Mingram B (1998) The Erzgebirge, Germany, a subducted part of northern Gondwana: geochemical evidence for repetition of early Palaeozoic metasedimentary sequences in metamorphic thrust units. Geol Mag 135(6):785–801

Mooney WD, Laske G, Masters TG (2008) CRUST 5.1: A global crustal model at $5° \times 5°$. J Geophys Res Solid Earth 103:727–747

Mrázová Š, Tomanová Petrová P, Krentz O (2020) Geologie des Sächsisch-Böhmischen Kreidebeckens zwischen Erzgebirge und Jeschken: ResiBil—Wasserressourcenbilanzierung und -resilienzbewertung im Ostteil des sächsisch-tschechischen Grenzraumes, Landesamt für Umwelt, Landwirtschaft und Geologie, Dresden

Nigro A, Sappa G, Barbieri M (2017) Strontium isotope as tracer of groundwater contamination. Proc Earth Planet Sci 17:352–355

Palmer MR, Edmond JM (1992) Controls over the strontium isotope composition of river water. Geochim Cosmochim Acta 56(5):2099–2111

Peterson EE, Ver Hoef JM (2014) STARS: An ArcGIS toolset used to calculate the spatial information needed to fit spatial statistical models to stream network data. J Stat Softw 56(2):1–17

Podio NS, Baroni V, Badini RG, Inga M, Ostera A, Cagnoni M, Gautier EA, García PP, Hoogewerff J, Wunderlin DA (2013) Elemental and isotopic fingerprint of argentinean wheat. Matching soil, water, and crop composition to differentiate provenance. J Agric Food Chemistry 61(16):3763–3773

Potter P, Ramankutty N, Bennett EM, Donner SDA (2010) Characterizing the spatial patterns of global fertilizer application and manure production. Earth Interact 14:1–22

Price TD, Burton JH, Bentley RA (2002) The characterization of biologically available strontium isotope ratios for the study of prehistoric migration. Archaeometry 44(1):117–135

Rajchl M, Uličný D, Mach K (2008) Interplay between tectonics and compaction in a rift-margin, lacustrine delta-system: Miocene of the Eger Graben, Czech Republic. Sedimentology 55:1419–1447

Rohde S (2014) Zusammenstellung geogener Hintergrundwerte in sächsischen Gewässern. Landwirtschaft und Geologie (LfULG), pp 30–39

Scaffidi BK, Tung TA, Gordon G, Alaica AK, González La Rosa LM, Marsteller SJ, Dahlstedt A, Schach E, Knudon KJ (2020) Drinking locally: a water $^{87}Sr/^{86}Sr$ isoscape for geolocation of archeological samples in the Peruvian Andes. Front Ecol Evol 8:281

Schneider JW, Rößler R, Fischer F (2012) Rotliegend des Chemnitz-Beckens. In: Lützner H, Kowalczyk G (eds) Stratigraphie von Deutschland X. Rotliegend. Teil I: Innervariscische Becken. Schriftenreihe der Deutschen Gesellschaft für Geowissenschaften, Heft vol 61, pp 530–588

Spiess H, and Geologisches Landesamt Sachsen-Anhalt (1998) Geologische Karte Harz. 1. Aufl. Geologisches Landesamt Sachsen-Anhalt, Halle

Thomsen E, Andreasen R (2019) Agricultural lime disturbs natural strontium isotope variations: implications for provenance and migration studies. Sci Adv 5(3):eaav8083

Tichomirowa M, Heidel C, Junghans M, Haubrich F, Matschullat J (2010) Sulfate and strontium water source identification by O, S and Sr isotopes and their temporal changes (1997–2008) in the region of Freiberg, central-eastern Germany. Chem Geol 276:104–118

Ulrych J, Dostal J, Adamovič J, Jelínek E, Špaček P, Hegner E, Balogh K (2011) Recurrent Cenozoic volcanic activity in the Bohemian Massif (Czech Republic). Lithos 123(1):133–144

Ver Hoef JM, Peterson EE, Clifford C, Shah R (2014) SSN: an R package for spatial statistical modelling on stream networks. J Stat Softw 56(3):1–45

Vet R, Artz RS, Carou S, Shaw M, Ro CU, Aas W, Baker A, Bowersox VC, Dentener F, Galy-Lacaux C, Hou A, Pienaar JJ, Gillett R, Forti MC, Gromov S, Hara H, Khodzher T, Mahowald NM, Nickovic S, Rao PSP, Reid NW (2014) A global assessment of precipitation chemistry and deposition of sulfur, nitrogen, sea salt, base cations, organic acids, acidity and pH, and phosphorus. Atmos Environ 93:3–100

Voerkelius S, Lorenz GD, Rummel S, Quétel CR, Heiss G, Baxter M, Brach-Papa C, Deters-Itzelsberger P, Hoelzl S, Hoogewerff J, Ponzevera E, Van Bocxstaele M, Ueckermann H (2010) Strontium isotopic signatures of natural mineral waters, the reference to a simple geological map and its potential for authentication of food. Food Chem 118(4):933–940

Voigt T (2004) Late Cretaceous unconformities in the Subhercynian Basin (Germany). Acta Geol Pol 54(4):673–694

West JB, Bowen GJ, Dawson TE, Tu KP (2010) Isoscapes—understanding movement, pattern, and process on Earth through isotope mapping. Springer, Dordrecht, p 487

Zech J, Jeffries T, Faust D, Ullrich B, Linnemann U (2010) U-Pb-dating and geochemical characterization of the Brocken and the Ramberg Pluton, Harz Mountains, Germany. Geologica Saxonica 56(1):9–24

Ziegler PA (1990) Geological atlas of western and Central Europe. Blackwell, Oxford

Zieliński M, Dopieralska J, Belka Z, Walczak A, Siepak M, Jakubowicz M (2018) Strontium isotope identification of water mixing and recharge sources in a river system (Oder River, central Europe): a quantitative approach. Hydrol Process 32(16):1–15

Zieliński M, Dopieralska J, Królikowska-Ciągło S, Walczal A, Belka Z (2021) Mapping of spatial variations in Sr isotope signatures ($^{87}$Sr/$^{86}$Sr) in Poland—implications of anthropogenic Sr contamination for archaeological provenance and migration research. Sci Total Environ 775:145792

**Publisher's Note**  Springer Nature remains neutral with regard to jurisdictional claims in published maps and institutional affiliations.